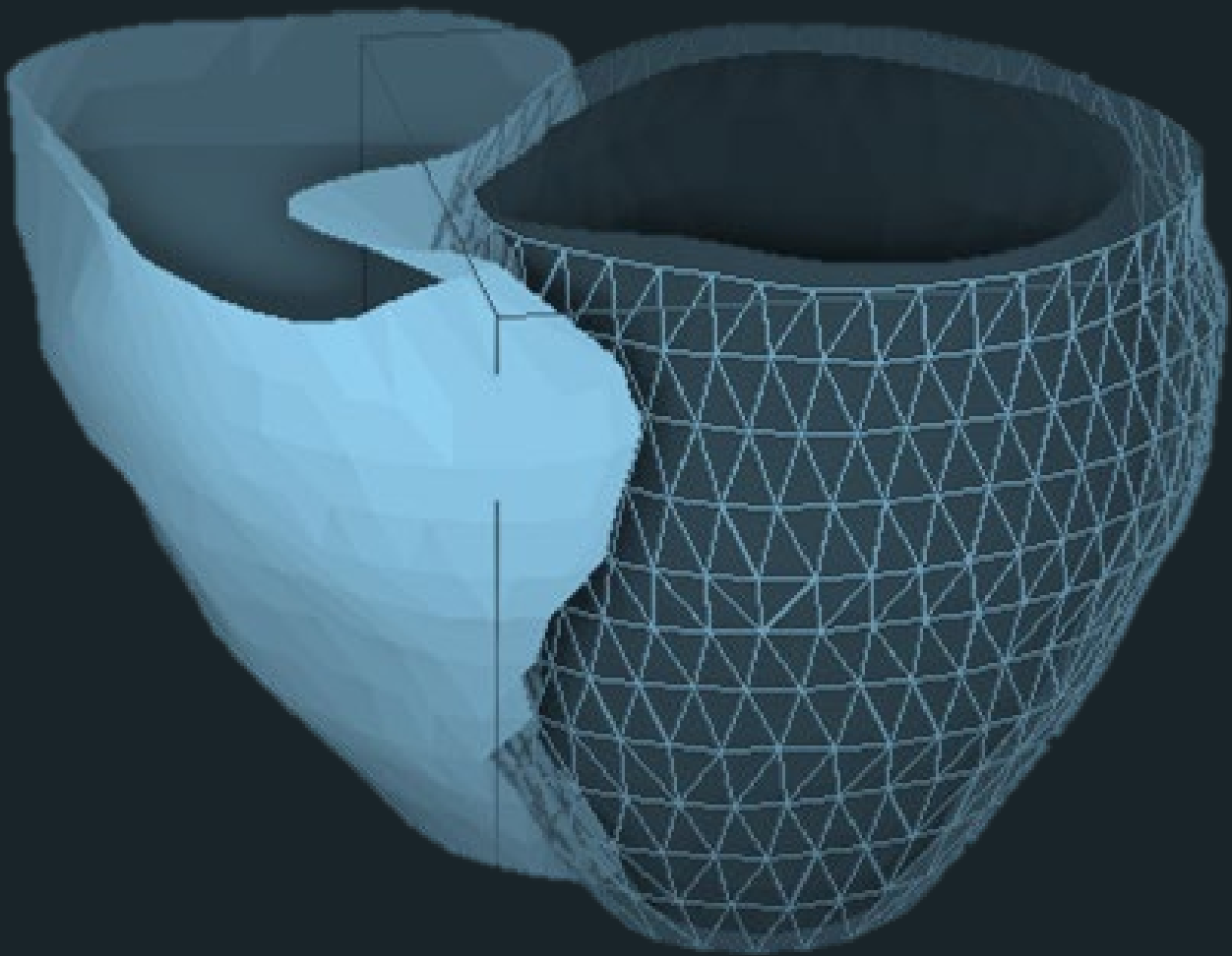# Diastolic strain rate for predicting mortality in kidney transplant recipients

MSc Thesis Technical Medicine

Daniek van der Kaaij
August 2023

Universiteit Leiden

TUDelft

Erasmus MC

DIASTOLIC STRAIN RATE BY CARDIAC MRI FOR PREDICTING MORTALITY IN KIDNEY TRANSPLANT RECIPIENTS

Daniek van der Kaaij

Student number: 4561104

21 August 2023

Thesis in partial fulfilment of the requirements for the joint degree of Master of Science in

Technical Medicine

Leiden University; Delft University of Technology; Erasmus University Rotterdam

Master thesis project (TM30004; 35 ECTS)

Dept. of Radiology, Leiden University Medical Center

Dept. of Nephrology, Leiden University Medical Center
January 2023 – September 2023

Supervisor(s):

Dr. I.A. Dekkers	Daily supervisor
Prof. dr. H.J. Lamb	Technical supervisor
Dr. A.P.J. de Vries	Medical supervisor

Thesis committee members:

Prof. dr. J.J. van den Dobbelsteen	Delft University of Technology (chair)
Dr. I.A. Dekkers	Leiden University Medical Center
Prof. dr. H.J. Lamb	Leiden University Medical Center
Dr. A. Ray	Leiden University Medical Center

An electronic version of this thesis is available at http://repository.tudelft.nl/.

Universiteit Leiden

TUDelft
Delft University of Technology

ERASMUS UNIVERSITEIT ROTTERDAM

Acknowledgements

Summary

High cardiovascular mortality primarily limits survival following kidney transplantation (KTx). The increased risk is intrinsically connected to cardiac structural and functional abnormalities. LV volumetric imaging measurements are commonly used to quantify this, such as left ventricular ejection fraction (LVEF) and left ventricular end-diastolic volume index (LVEDVi). However, there is an increasing interest in the assessment of myocardial strain. It provides direct information about myocardial function by measuring the deformation of myocardial fibres during the cardiac cycle.

An impaired LV diastolic strain is associated with adverse outcomes in end-stage kidney disease (ESKD) patients. Cardiac magnetic resonance imaging (MRI) has emerged as the golden standard for evaluating cardiac structure and function. However, studies investigating the prognostic value of myocardial strain are mainly based on echocardiography, and diastolic strain still needs to be examined in KTx recipients.

Chapter 1 hypothesized that myocardial strain has the potential to detect early diastolic dysfunction more effectively when compared to LV volumetric measurements. The primary objective of this thesis was to determine whether it is possible to predict all-cause mortality of KTx recipients on cardiac MRI two weeks post-KTx by diastolic strain.

Chapter 2 presents the technical background of myocardial strain imaging. The principles of cardiac MRI feature tracking and resulting outcomes are explained. Subsequently, methods implemented in the feature tracking software package Medis Suite MR are described.

The methods of this thesis are in described in Chapter 3. Data from patients included in the Amsterdam Leiden GROningen (ALEGRO) trial were used. Medis Suite MR was used to calculate LV volumetric outcomes and identify deformation of the LV during the cardiac cycle. A MATLAB script was developed to obtain diastolic strain rate outcomes from these data. Kaplan-Meier curves were used for survival analysis and Cox regression analysis was performed to identify independent predictors of survival.

Chapter 4 presents the results of the strain and survival analysis. 67 patients were included with cardiac MRI at baseline, two weeks post-KTx. The mortality was 27% (n=18) over a median follow-up of 10 years. Significant differences between survival distributions were found based on longitudinal peak early diastolic strain rate (PEDSR) at baseline. Using LV volumetric outcomes, including LVEF, LVEDVi and left ventricular end-systolic volume index (LVESVi), this was achievable starting from a follow-up of one year. Multivariable analysis showed that longitudinal PEDSR was the strongest independent predictor of mortality at baseline.

The interpretation of the results and concluding remarks of this theses are discussed in Chapter 5. It is demonstrated that myocardial strain has the potential to detect early diastolic dysfunction more effectively when compared to LV volumetric outcomes. Longitudinal PEDSR measured two weeks post-KTx by cardiac MRI independently predicts all-cause mortality and provides incremental prognostic information beyond clinical parameters. Further research in cardiovascular therapeutics is an essential next step in improving KTx recipients' prognosis.

Contents

1

Introduction

1.1. Clinical context

Patients with end-stage kidney disease (ESKD) have a significantly increased risk of cardiovascular disease (CVD) compared to the general population [1]. Kidney transplantation (KTx), the preferred treatment for eligible ESKD patients, reduces this risk compared to patients receiving dialysis treatment. However, survival post-KTx is still primarily limited by high cardiovascular mortality [1, 2].

The increased risk of CVD is intrinsically connected to cardiac structural and functional abnormalities [1]. Uraemic cardiomyopathy is the term used to describe cardiovascular abnormalities associated with ESKD and is classically characterized by left ventricular hypertrophy, in addition to both systolic and diastolic dysfunction [3]. LV volumetric imaging measurements are commonly used to quantify this, such as left ventricular mass index (LVMi) and left ventricular ejection fraction (LVEF).

In addition to the volumetric analysis of left ventricle (LV) function, there is an increasing interest in quantifying myocardial strain. Strain measurements provide direct information about myocardial function by measuring the deformation of myocardial muscle fibres during the cardiac cycle and may be more sensitive to early subclinical myocardial dysfunction [4, 5]. The previously conducted literature study for this thesis compared myocardial strain with LV volumetric measurements as potential early markers of reversal of uraemic cardiomyopathy following KTx. It was shown that systolic strain, including global circumferential strain (GCS) and global radial strain (GRS), but not global longitudinal strain (GLS) improved after KTx, indicating a reversal of uraemic cardiomyopathy. However, only the effects of KTx on systolic strain were examined, while diastolic strain is also important to consider.

Uraemic cardiomyopathy is also characterized by diastolic dysfunction, which may be important for the prognosis of KTx recipients [6, 7]. In ESKD patients, LV hypertrophy can cause increased myocardial energy deficits and interstitial fibrosis [5]. It is increasingly being recognized that the degree of myocardial fibrosis correlates strongly with the development of arrhytmia and sudden cardiac death [6]. Fibrosis makes the heart muscle less flexible, hindering its ability to relax during diastole and decreasing the diastolic strain rate. Previous literature has also indicated the diagnostic value of LV diastolic strain rate. Impaired LV myocardial strain can be used as a predictor of adverse cardiovascular outcomes and all-cause mortality in ESKD patients [8–11]. Early detection of diastolic dysfunction may prompt earlier changes in pharmacological treatment to minimize irreversible myocardial fibrosis and improve prognosis [12].

Cardiac MRI has emerged as the golden standard for evaluating cardiac structure and function. However, studies investigating the prognostic value of myocardial strain in ESKD patients are mainly based on echocardiography [8–11, 13, 14]. Only Rankin et al. assessed the association between myocardial strain and the mortality risk in ESKD patients by cardiac MRI [1]. However, this study did not specifically include KTx recipients and the diastolic strain was not examined. Therefore, there is a need to study the prognostic value of diastolic strain in KTx recipients by cardiac MRI.

1.2. Project aim

It is hypothesized that myocardial strain has the potential to detect early diastolic dysfunction more effectively when compared to LV volumetric measurements. The primary objective of this thesis is to determine whether it is possible to predict all-cause mortality of KTx recipients on cardiac MRI two weeks post-KTx by diastolic strain. The Amsterdam LEiden GROningen (ALEGRO) trial provides a unique clinical setting in which this can be assessed as patients were subjected to cardiac MRI following KTx.

2

Technical background

In this chapter, the technical background of myocardial strain analysis is presented. First, the concepts of myocardial strain and related measurements are introduced. This is followed by the principles of cardiac MRI feature tracking, used for strain calculation. Lastly, the methodology integrated into the Medis software is described.

2.1. Myocardial strain

Myocardial strain measures deformation of myocardial muscle fibres during the cardiac cycle. The deformation is quantified by comparing the length of muscle fibres at the end-systolic phase to their length at the end-diastolic phase. This reflects how much they have shortened or lengthened, providing direct information about the myocardial contraction and relaxation.

The deformation can be quantified in three different directions: longitudinal, circumferential and radial. Longitudinal and circumferential strain represent shortening of the myocardium and are thus negative, with lower values indicating better function. Conversely, radial strain values represent stretching and are normally positive, with higher values indicating better function.

Ventricle strain values are determined in each heart segment (Figure 2.1) and subsequently averaged to obtain global strain values. GLS, GCS and GRS are three measurements of systolic myocardial strain (Figure 2.2). Strain measurements are expressed as percentage as they reflect proportional changes in cardiomyocyte length. Commonly used measurements points along strain curves are:

1. End-systolic (ES) strain: the value at end-systole.

2. Peak systolic strain: the peak value during systole.

3. Peak strain: the peak value during the entire heart cycle, which may coincide with the ES or peak systolic strain, or may appear after aortic valve closure (post-systolic strain).

Secondly, strain rate (1/s) is the first derivative of strain, measuring the rate at which deformation of the myocardial muscle fibres occurs during the cardiac cycle. High absolute strain rate values typically indicate increased deformation, which could suggest forceful cardiac contractility and effective relaxation. In Figure 2.3, strain rate points that can be measured along strain rate curves are displayed:

1. Peak systolic strain rate (PSSR): maximum strain rate during systole caused by ventricular contraction.

2. Peak early diastolic strain rate (PEDSR): first peak in diastole caused by ventricular relaxation.

3. Peak late diastolic strain rate (PLDSR): second peak in diastole caused by atrial contraction.
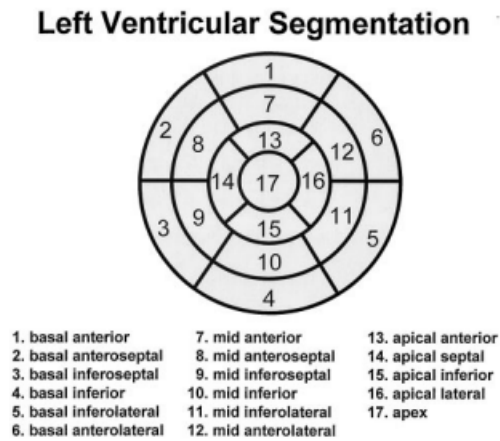
Figure 2.1: Display, on a circumferential polar plot, of the 17 myocardial segments and the recommended nomenclature for tomographic imaging of the heart [15].
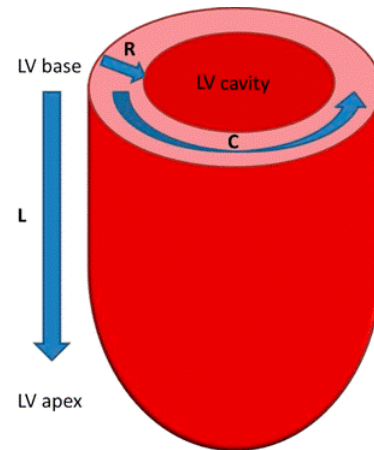
Figure 2.2: Graphical representation of ventricular strain measurements [16]. C, global circumferential strain; L, global longitudinal strain; R, global radial strain; LV, left ventricle.

2.2. Cardiac MRI feature tracking

In this thesis, the cardiac MRI feature tracking software package Medis Suite MR (Version 4.0.56.4) will be used to calculate global strain values. Cardiac MRI feature tracking is based on optical flow technology to measure motion in cardiac images. It involves tracking specific features or regions of interest within sequential image frames to determine their displacement over time (Figure 2.4). In cardiology, features should ideally have a size equivalent to a few pixels to be identifiable, while the window size used for analysis should be at least 8 x 8 pixels [18].

The displacement of features or regions (ΔL) is specified as the distance between length in the end-diastolic (L0) and end-systolic phase (L1) (Figure 2.4).Subsequently, the Lagrangian strain (%) is calculated from the displacement according to the following formula:

$$\text{Lagrangian strain} = \frac{L1 - L0}{L0} = \frac{\Delta L}{L0} \tag{2.1}$$
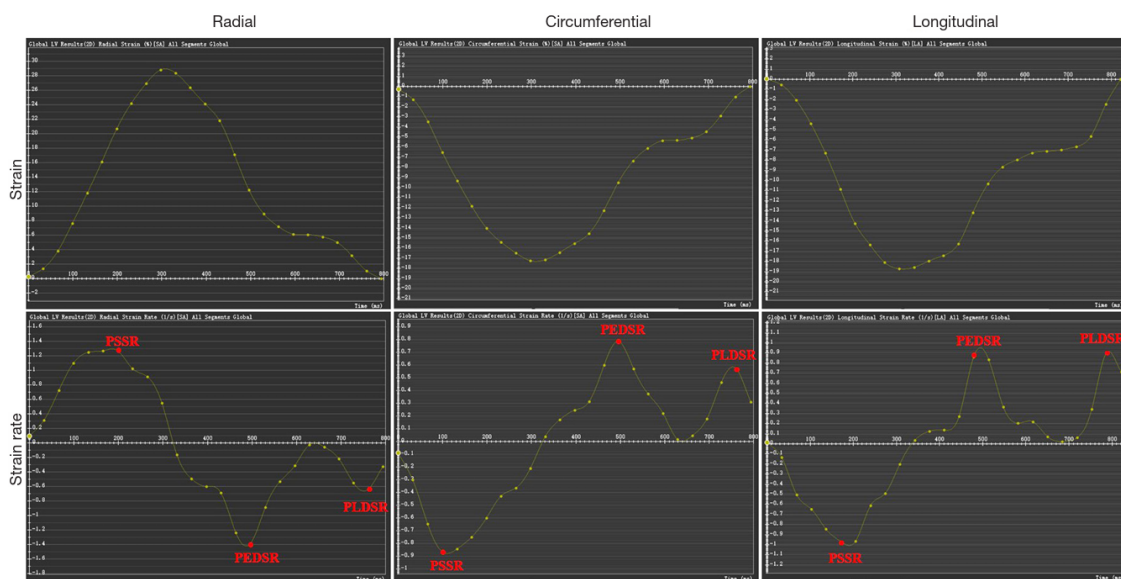
Figure 2.3: Example of left ventricle strain and strain rate graphs in three directions [17]. PSSR, peak systolic strain rate; PEDSR, peak early diastolic strain rate; PLDSR, peak late diastolic strain rate.

Regularization and strain computation — **Matched pattern** — **Template and pattern search** — **Template and pattern selection**

Figure 2.4: Principle of feature tracking on cardiac MRI. trace points at the endocardial border are identified and followed over time in the subsequent images by searching the most likely pattern match. Adapted from Amzulescu et al. [19].

Lagrangian strain rate (1/s) is the first derivative of strain:

$$\text{Lagrangian strain rate} = \frac{1}{L0}\frac{dL(t)}{dt} = \frac{\Delta L}{L0} \tag{2.2}$$

Strain values describe the lengthening or shortening of myocardial tissue in three directions (longitudinal, circumferential and radial). These three principal strains represent the 3D deformation of the heart without any shearing [18].

Lagrangian strain relates the deformation always to the baseline length (L0). On the other hand, when calculating natural strain the reference length is always changing. It therefore describes the instantaneous length change. However, with feature tracking this is not convenient since the baseline length is always known and can easily be used as a reference.

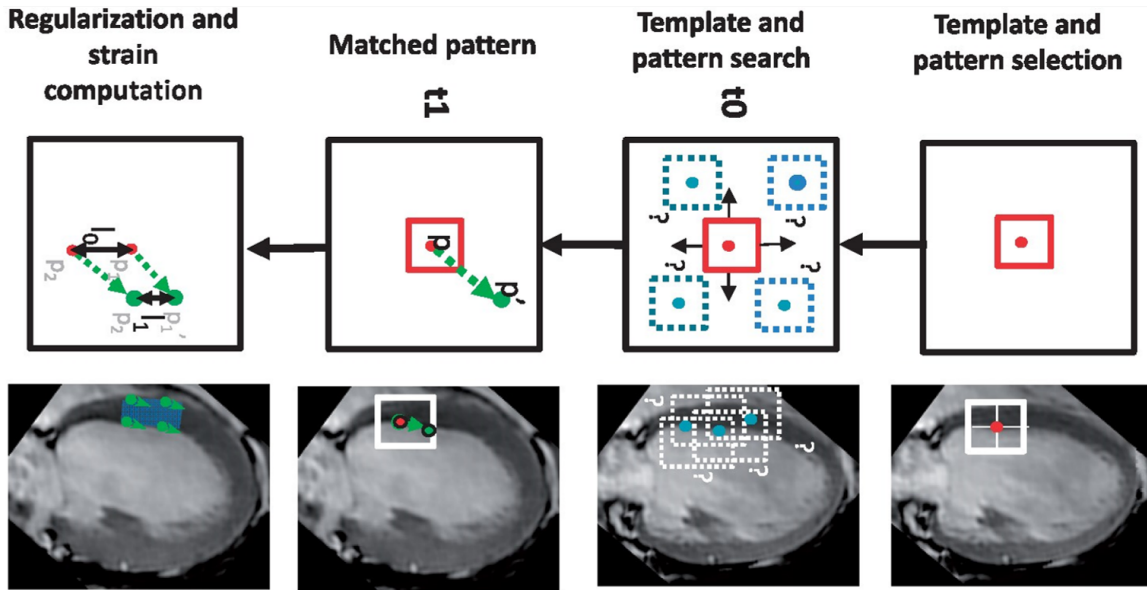### 2.2.1. Global strain analysis in Medis

This section explains the methods integrated into Medis to determine global strain values. Longitudinal strain is computed based long axis (LAX) on 2, 3- or 4- chamber views, while radial and circumferential strain require the use of short axis (SAX) series. For circumferential and radial strain, slices are selected at the level of the mitral valve, papillary muscle and apex.

To track the deformation of the left ventricle, the first step is to identify the endocardial and/or epicardial contours at the end-systolic and end-diastolic phase. A deep learning-based method, is implemented for this, however, contours can be checked and edited manually [20]. Subsequently, 48 trace points at the myocardial-cavity boundary are tracked throughout the cardiac cycle by searching the same regions in the following frames. Within every cardiac phase, the displacement of individual trace points is represented by arrows, with the orientation and length of each arrow corresponding to the displacement (Figure 2.5). Medis saves all outcomes in data sheets, where trace points are stored as rows and cardiac phases as columns.

The 17-segment model is used for LAX and the 16-segment model for SAX series. Calculations of the individual segments (Figure 2.1) are done based on different views or slices. The 2-chamber view is used for segment 1, 4, 7, 10, 13, 15 and 17, the 3-chamber view for segment 2, 5, 8 and 11, and the 4-chamber view for segment 3, 6, 9, 12, 14, 16 and 17. The SAX slice at the level of the mitral valve corresponds to the six basal segments (1-6), the papillary muscle to the mid segments (7-12) and the apex to the

apical segments (13-16). In each slice, the 48 trace points Figure 2.5 are divided over the corresponding segments. For example, to each segment at the slice at the level of the mitral valve belong eight trace points (48 divided by six segments). At each cardiac phase, the mean of these eight trace points is the resulting displacement of that specific basal segment.

Based on the displacements, the strain can be determined in three directions. Initially, the strain is determined at the end-systolic phase on a segmental basis. When evaluating global strain, the values from all segments are averaged. Segmental strain rates can also be obtained in Medis, however strain rates averaged over all segments are not provided.
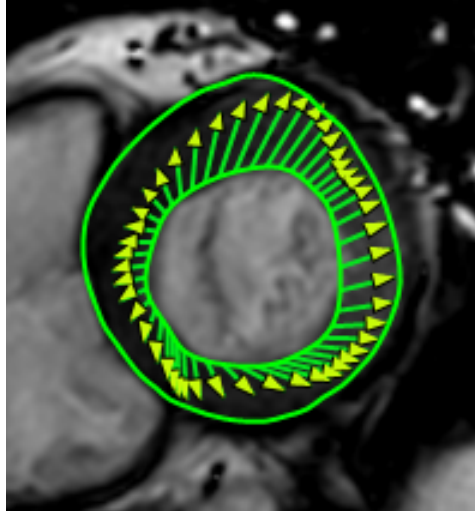

Figure 2.5: 48 trace points at the endocardial border used for strain analysis, with the orientation and length corresponding to their displacement.

3

Methods

In the next chapter, information about the included study population and clinical data collection is described, which is followed by the image acquisition. After that, a detailed step-by-step explanation of the image and statistical analysis is provided.

3.1. Study population

This thesis was a multi-center retrospective study, conducted at the cardiovascular imaging group of the Leiden University Medical Center (LUMC). Patients in the ALEGRO trial who also underwent cardiac MRI were included for this additional analysis. Cardiac MRI was performed either at the LUMC or Amsterdam Medical Center (AMC). The ALEGRO trial divided patients into three groups: the steroid-free group (1a), standard group (2a), and the low-dose calcineurin inhibitor (CNI) group (2b). Detailed information about the ALEGRO trial's protocol can be found in Appendix A. Patients have given informed consent and approval from the Medical Research Ethics Committee (MREC) of the LUMC and AMC has been obtained.

3.2. Clinical data collection

The clinical data of patients was obtained in two ways. First, the already existing trial database could be used to copy some variables from. All remaining variables were retrieved from patients electronic medical records if available. Patient data were anonymized and recorded in an Excel database (Version 2306). Data closest to the day of the first cardiac MRI scan were used.

The clinical data included demographic characteristics (age, sex, body height, body mass index (BMI) and body surface area (BSA)), primary diagnosis (diabetes mellitus (DM) type II/hypertension/ glomerulonephritis/autosomal dominant polycystic kidney disease (ADPKD)/focal segmental glomerulosclerosis (FSGS)/other), dialysis details (preemptive/hemodialysis/peritoneal dialysis/ both, duration and the presence of an arteriovenous (AV) fistula), renal risk factors (history of CVD, hypertension, systolic blood pressure (SBP) and DM), transplantation information (first/second kidney transplant and living/postmortal donor), as well as biochemical measurements (tacrolimus, high sensitive C-reactive protein (CRP), creatine clearance, hematocrit and haemoglobin) and virology (Epstein-Barr virus (EBV) and cytomegalo virus (CMV) status of donor and acceptor). Further, the number and cause of death was collected.

3.3. Image acquisition

Cardiac MRI was performed between January 2012 and December 2017. At the LUMC, scans up to March 2013 were scanned on a Philips 1,5T scanner, hereafter on 3T. The AMC patients were first scanned on Philips 1.5T as well, and on 3T from December 2014. Patients were scanned at two weeks, twelve and 24 months post-KTx, hereafter referred to as baseline (BL), follow-up at one year (FU1) and follow-up at two years (FU2).

The cardiac cycle of the patients in the LUMC was typically scanned using sixteen slices and 35 phases. On the other hand, the patients at the AMC underwent cardiac scans with twelve slices and forty phases. All images were obtained with breath-hold at end-expiration. Standard 2- and 4-chamber balanced steady-state free precession (bSSFP) cine images for LV analysis were acquired with the following parameters: slice thickness 8 mm, field of view 350 mm, flip angle 45 degrees, repetition time 2.8-3.0 s, echo time 1.38-1.5 ms and matrix size 176 x 176 or 232 x 219.

3.4. Image analysis

The workflow for calculating the results for each patient at all time points is illustrated in Figure 3.1. First, the cardiac MRI of the patients were retrieved from PACS using the Sectra IDS7 PACS workstation (Sectra Imtec AB, Linköping, Sweden). Scans from the AMC were directly imported from the local disk.

In Medis Suite MR (Version 4.0.56.4, Medis Medical Imaging Systems, Leiden, The Netherlands), two software applications were used. Initially, QMass was used to automatically detect LV contours, allowing a quantitative assessment of ventricular function. Subsequently, QStrain was used to analyze deformation during the cardiac cycle. To also obtain strain rate results, the data was exported to MATLAB (R2022b). All steps in QMass, QStrain and MATLAb are explained in the following sections.
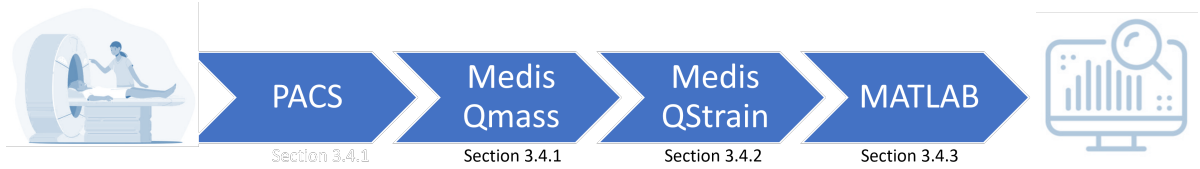
Figure 3.1: Schematic overview of the workflow for obtaining cardiac MRI strain results.

3.4.1. Medis QMass

The cardiac MRI imaging of a specific patient and time point was accessed from the Medis repository. The SAX and 2- and 4-chamber cine views were used for further analysis. For each view, the QMass application was started to perform automatic LV contour detection, facilitating the acquisition of structural and functional LV measurements. In QMass, the first step was to select the 'MassK' checkbox. This ensured exclusion of papillary muscles and trabeculae. The LV threshold of MassK was left at the default of fifty to distinguish blood from muscle [17].

Prior to this, the AutoQ algorithm had been activated to preprocess newly arrived data in the repository. In this way, LV contours should be automatically identified in the end-diastolic and end-systolic phase in the incoming cine series. The AutoQ algorithm preprocesses these series in the background, without requiring any user input. To detect LV contours automatically, a deep learning-based method was implemented in Medis [20]. The contours were manually checked edited manually if necessary.

Unfortunately, imported cine series were often not recognized by the AutoQ algorithm. Therefore, the end-diastolic and end-systolic phases had to be manually marked in most cases. A representative example of the resulting LV contours can be seen in Figure 3.2.

After segmenting the LV in each short-axis slice, LV volumtric variables were calculated. For the LV volume at end-diastole (LVEDV) and end-systole (LVESV), the volumes at these two phases were summed for all segmented slices. The LVM was determined by multiplying the slice thickness and interslice distance with the area enclosed between the endocardial and epicardial boundaries in consecutive short-axis slices during end-diastole [21]. Additionally, the LVM/EDV was determined as this variable was associated with diastolic dysfunction [22, 23]. left ventricular end-diastolic volume indexed (LVEDVi) and left ventricular end-systolic volume indexed (LVESVi) were indexed by dividing by the patient's body surface area (BSA), LVM by dividing by the body height to the power of 2.7. The cardiac output, which is the product of the heart rate and stroke volume, was normalized to the BSA as well. The LVEF was calculated as follows:

$$LVEF = (LVEDV - LVESV)/LVEDV * 100\%\qquad(3.1)$$
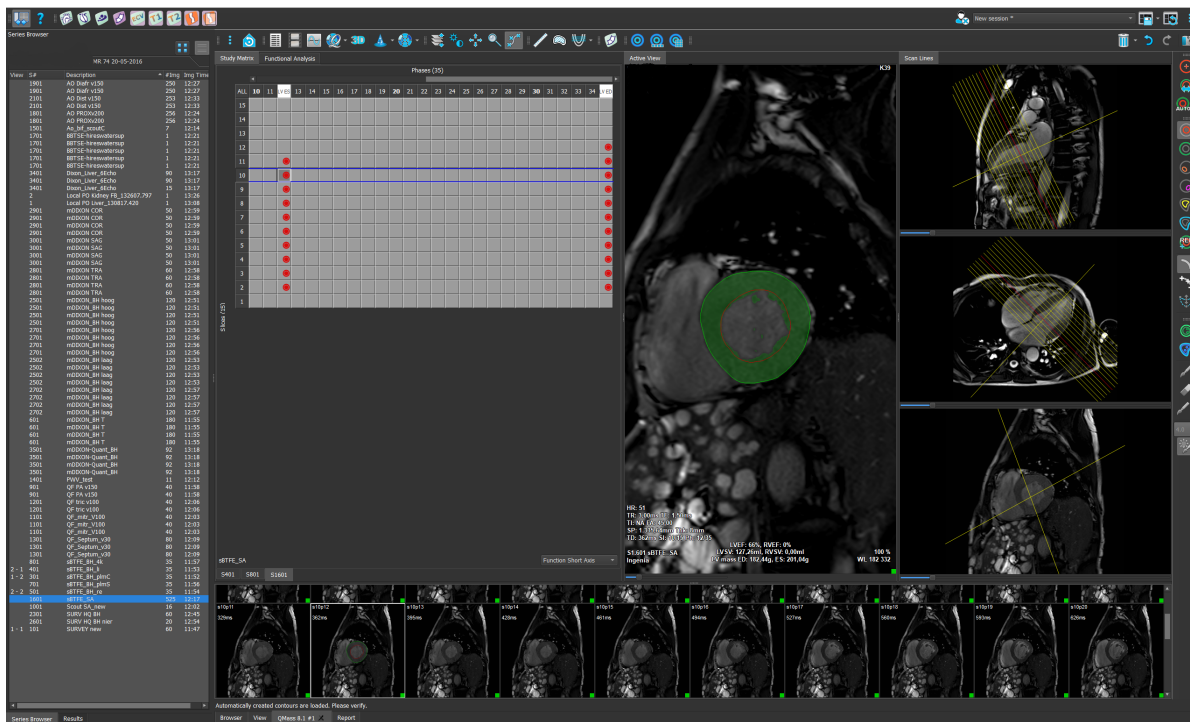
Figure 3.2: Representative example of LV contour detection using QMass on short-axis cine imaging for a single patient.

Finally, the myocardial contraction fraction (MCF) was calcualted as it showed associations with adverse outcomes in earlier studies [24, 25]. The MCF was calculated by dividing the stroke volume (SV) by the myocardial volume. The myocardial volume, in turn, was determined by dividing the LVM by the myocardial density (1.05 g/mL). Of each variable, the mean and standard deviation per study group and time point was calculated (Table 3.1).

Table 3.1: Overview of LV volumetric outcomes at baseline and follow-up imaging.

	Abbreviations	Variables	Units
Structural	LVMi	Left ventricular mass index	g/m^2
	LVEDVi	LV volume at end-diastole index	mL/m^2
	LVESVi	LV volume at end-systole index	mL/m^2
Functional	CI	Cardiac index	L/min/m^2
	LVEF	Left ventricular ejection fraction	%
	MCF	Myocardial contraction fraction	%
	LVM/EDV	LVM divided by EDV	unitless

3.4.2. Medis QStrain

The QStrain application in Medis Suite uses cardiac MRI feature tracking for strain analysis, see Chapter 2. It enables the quantification of global and regional strain (Figure 3.3). QStrain can be started as an independent application or an integrated component of QMass. Launching from QMass is preferred because the created LV contours are then directly taken over.

Radial and circumferential strain are computed based on SAX series, while longitudinal strain requires the use of 2- or 4-chamber views. To initiate the SAX strain analysis, SAX slices at the level of the mitral valve, papillary muscle and apex were placed within their corresponding boxes. For LAX strain analysis, this was done with the 2- and 4- chamber views. In Medis, only the results of global and regional systolic strain are shown. Data sheets containing these raw results for each patient at different time points (BL, FU1 and FU2) were saved in local folders.

Figure 3.3: Example of LV global strain analysis using QStrain on short-axis cine imaging for a single patient.

3.4.3. MATLAB

To also obtain global strain rate, a MATLAB script was written. In this way, the LV strain outcomes for all patients could be automatically determined at the three time points (Table 3.2). The MATLAB script uses the data sheets exported from QStrain and similar methods to Medis, see Chapter 2.
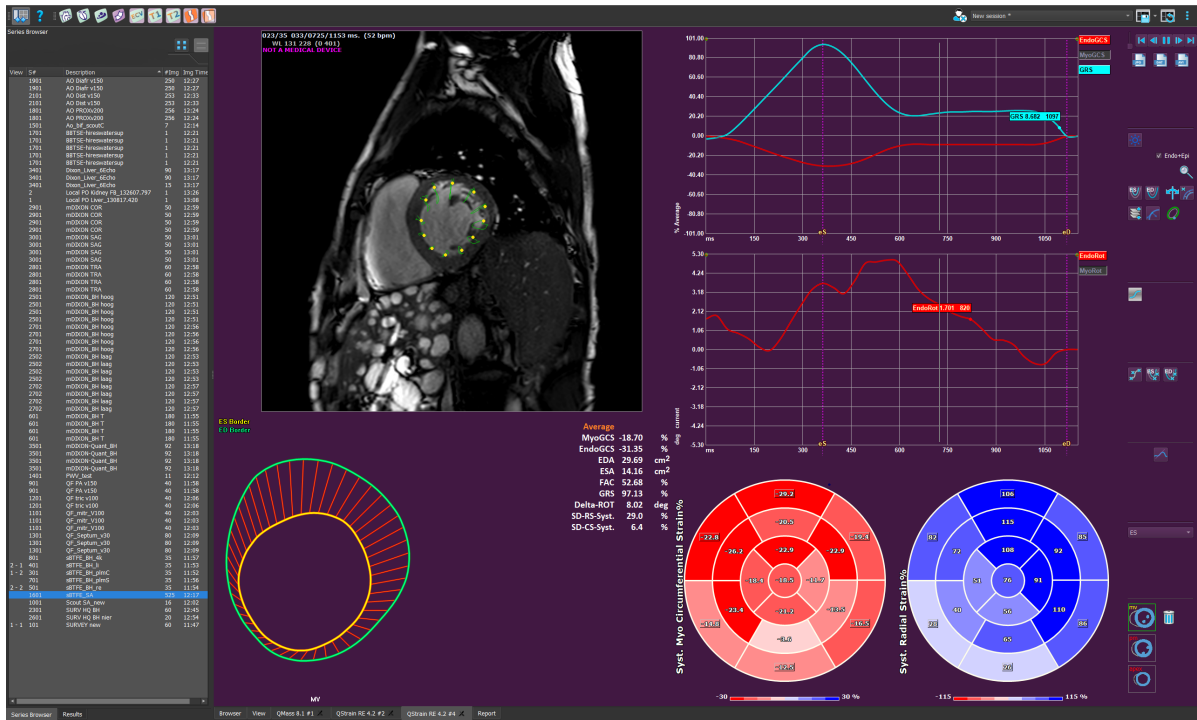
For longitudinal strain (rate), the average of the segments in the 2- and 4- chamber view was calculated. If the 2- or 4-chamber view was missing, only seven segments instead of thirteen were averaged. For radial and circumferential strain (rate), seventeen segments at the level of the mitral valve, papillary muscle and apex were averaged. The standard deviations for LAX and SAX analysis were calculated based on means of the 2- and 4- chamber views or slices at the mitral valve, papillary muscle and apex, respectively.

It was chosen to use endocardial instead of epicardial strain values. Endocardial values were considered to be more clinically relevant compared to epicardial values and most suitable for the early detection of cardiac abnormalities. The subendocardial layer is particularly sensitive due to its higher metabolic demands and vulnerability to insufficient blood supply. However, it is important to note that endocardial strain will result in higher results compared to epicardial strain values [19].

Secondly, strain values at the ES phase are used in subsequent analyses. This is recommended in the initiative to standardize deformation imaging by the European Association of Echocardiography (now European Association of Cardiovascular Imaging (EACVI)) and the American Society of Echocardiography (ASE) [26]. Strain at the ES phase is more intuitive because it capture an easily identifiable moment in the cardiac cycle. However, peak global systolic strain values were also calculated in MATLAB for comparison (Figure C1). The ES values consistently resulted in larger values, emphasizing the importance of labelling reported outcomes in a way that the definition of the parameter is clear.

The MATLAB function 'findpeaks' was used to identify the global strain, PSSR and the PEDSR. The PSSR represents the maximum strain rate during systole, indicating the maximum contraction of the ventricles. PEDSR corresponds to the first peak in diastole, reflecting passive ventricular deformation. It provides insights into the ventricle's ability to relax and fill adequately.
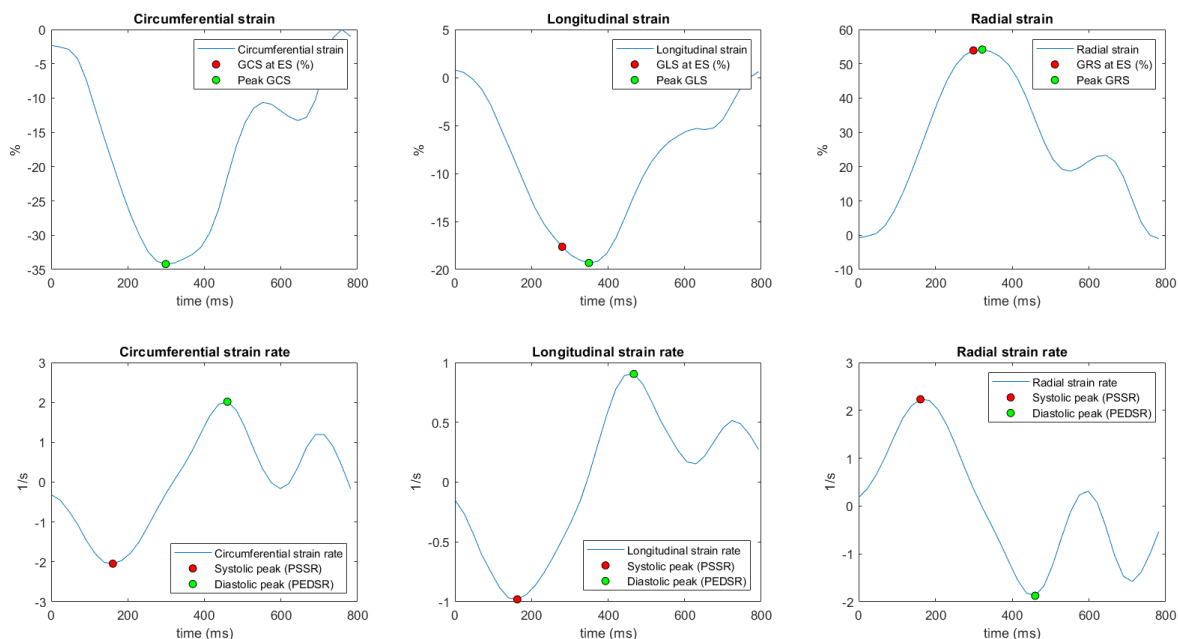
Figure 3.4: Representative example of strain (rate) analysis by using MATLAB at cardiac MRI (short-axis views and 2- and 4-chamber views) in three directions. GCS, global circumferential strain at end-systole (ES); GLS, global longitudinal strain at ES; GRS, global radial strain at ES; PSSR, peak systolic strain rate; PEDSR, peak early diastolic strain rate.

All strain measurements were calculated for all time points in three directions: circumferential, radial and longitudinal (Figure 3.4, Table 3.2). Outcomes were analyzed for all patients individually, and the mean and standard deviation for the entire group and for each study group were calculated.

Table 3.2: Overview of LV strain outcomes measured at baseline and follow-up imaging.

	Outcomes	Abbreviations
Global strain (%)	GCS	Global circumferential strain at end-systole
	GRS	Global radial strain at end-systole
	GLS	Global longitudinal strain at end-systole
Strain rate (1/s)	cPSSR	Circumferential peak systolic strain rate
	rPSSR	Radial peak systolic strain rate
	lPSSR	Longitudinal peak systolic strain rate
	cPEDSR	Circumferential peak early diastolic strain rate
	rPEDSR	Radial peak early diastolic strain rate
	lPEDSR	Longitudinal peak early diastolic strain rate

3.5. Statistical analysis

After the assessment of normal distribution with the Shapiro-Wilk test, normally distributed continuous baseline characteristics were shown as mean±standard deviation (SD) and non-normally distributed continuous variables were shown as medians with interquartile range (IQR). Categorical variables were represented as absolute numbers and percentages. Imaging outcomes were presented as means with the IQR. Statistical testing was performed using SPSS version 28.0.1 (SPSS Inc., Chicago, IL, USA). P-values <0.05 were considered statistically significant.

Baseline characteristics of surviving patients were compared to those who were deceased at follow-up. Comparison of continuous parametric data was performed by the Students t-test and non-parametric data using MannWhitney test. Categorical variables were compared using the Chi-square test. Changes in variables over time were analyzed with analysis of variance (ANOVA) with repeated measures and Bonferroni adjustment. One-way ANOVA was used for differences between groups (surviving/deceased and ALEGRO group 1/2a/2b). Outcomes were analyzed on an intention-to-treat basis.

Using receiver operating characteristic (ROC) curve analysis, each imaging outcome was compared by assessing the area under the curve (AUC) to identify a survival predictor. Optimal cutoff values were determined as the point where sensitivity and specificity had the highest combined value. Imaging outcomes with an AUC > 0.6 were used in the Kaplan-Meier survival analysis. Cox regression analysis was performed to identify independent predictors of survival. Variables with a p-value <0.20 in univariable analysis, together with the predefined clinical variables sex, AV-fistula and dialysis duration, were incorporated into the multivariable analysis, and a backward stepwise elimination approach was employed. In this way, potential predictors of all-cause mortality of KTx recipients can be identified.

To determine the intra-observer reproducibility of strain measurements, fifteen random cardiac MRIs (3T) were reanalyzed by the same observer. The intra-class correlation coefficient (ICC) (model, two-way mixed; type, absolute agreement) with 95% confidence interval (95% CI) were calculated. ICC values >0.75 indicated an excellent agreement, according to Cicchetti's guidelines [27].

4

Results

Chapter 4 provides the results of this thesis. First, the baseline characteristics of included patients are presented. The outcomes of image analysis, including LV volumetric, strain and strain rate, results are analyzed for all, and surviving/deceased patients separately. Subsequently, potential predictors of all-cause mortality of KTx recipients are identified based on cardiac MRI two weeks post-KTx, which was the primary objective of this thesis. Additionally, differences between the three ALEGRO groups are analyzed and the intra-observer variability of strain measurements is evaluated.

4.1. Study population

In the ALEGRO trial, 305 patients were initially randomized (Figure 4.1). 297 patients were included, with 98 assigned to group 1 (steroid-free) and 199 to group 2 (standard). The total number of patients with cardiac MRI available at baseline (two weeks post-KTx) was 67 (20 from group 1 and 47 from group 2). After six months, group 2 was divided into subgroups 2a and 2b (low-dose CNI). At follow-up at one year, fifty patients had cardiac MRI available (fifteen from group 1, nineteen from group 2a, and sixteen from group 2b). By the end of the study (at two years), cardiac MRI was performed of 38 patients (eleven patients from group 1, thirteen patients from group 2a, and fourteen patients from group 2b).

Table 4.1 summarizes the baseline characteristics of patients with cardiac MRI. The mortality was 27% (n=18) over a median follow-up of 10 years. A specific cause of death was available for eleven (61%) patients and included seven (64%) due to cancer, three due to pulmonary infection (27%) and one (9%) of a complication after hip fracture. Compared to surviving patients, deceased patients were older (65.5 [57.0-69.8] versus 58.0 [49.0-92.4] years; P<0.001), more likely to have CVD (50% versus 2%; p = 0.017) and igG positive EBV status at baseline (100% versus 78%; p = 0.028). Other characteristics were well balanced between both groups. The median tacrolimus (tac) trough levels were within the predefined boundaries of 8 to 12 ng/mL.
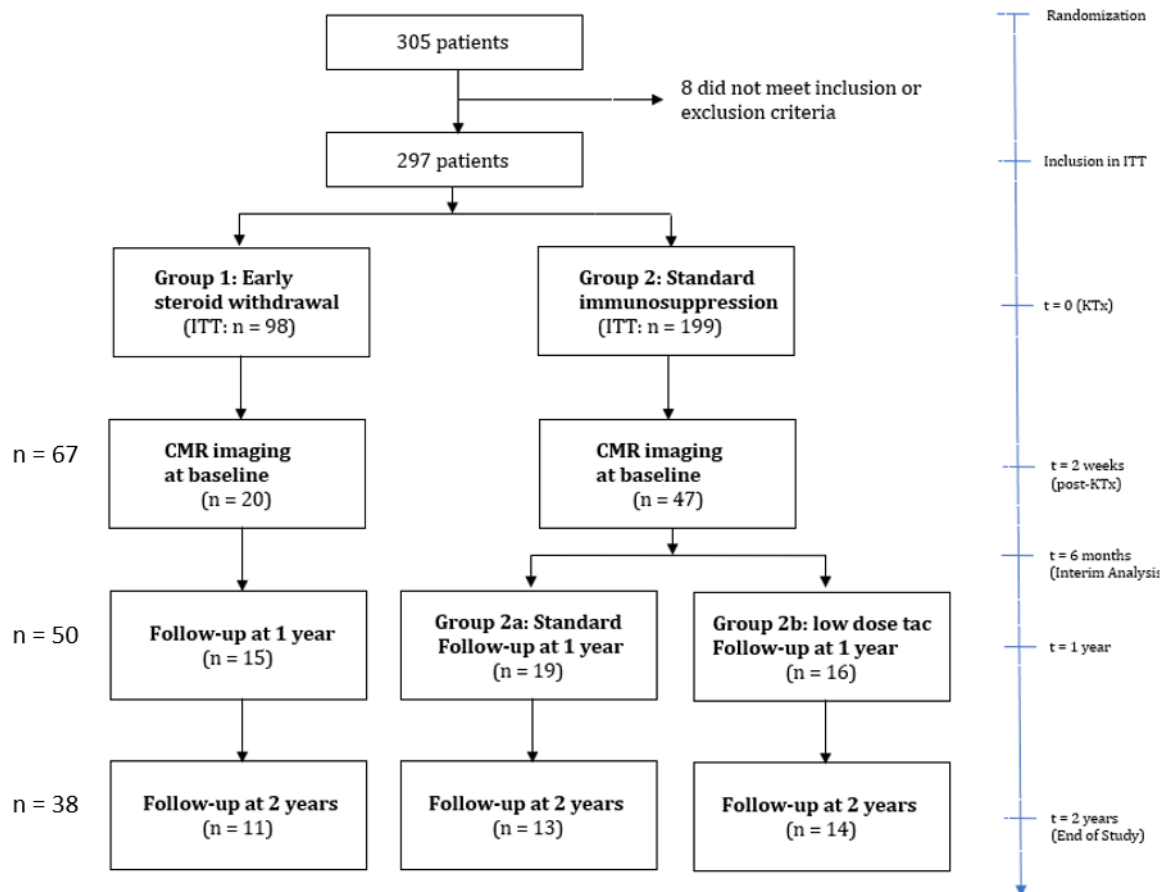
Figure 4.1: Schematic overview of ALEGRO enrollment and follow-up with cardiac MRI. Group 1: Standard tacrolimus (tac) + mycophenolic acid (MMF); Group 2(a): Standard tac/MMF/prednisolone (pred); Group 2b: Low tac/MMF/pred. MRI, magnetic resonance imaging; ITT, intention-to-treat; KTx, kidney transplantation.

4.2. Image analysis

A total of 155 scans were included in the analysis. Among these, 32 scans were conducted at the AMC, with 24 scans performed on a 1.5T scanner and eight on a 3T scanner. At the LUMC, only nineteen of the 123 scans were performed on a 1.5T scanner.

4.2.1. LV volumetric outcomes

The volumetric imaging outcomes at three time points are available in Table 4.2. The LVEF and LVM/EDV were above normal ranges, whereas the LVEDVi was below the normal mean value [Zhan]. The LVM was indexed by dividing by the body height to the power of 2.7, which, upon initial observation, leads to small values. However, when comparing to normal ranges they do not indicate LV hypertrophy [28].

One way ANOVA with repeated measures and Bonferroni adjustment revealed that LVMi, CI and LVEDVi differed significantly between time points. LVMi ($p = 0.004$) and LVEDVi ($p = 0.041$) decreased from baseline to FU2 in all patients. The LVMi was also significantly decreased from BL to FU2 in surviving patients ($p > 0.001$). CI decreased from baseline to FU1 ($p = 0.036$) and FU2 (< 0.001) in all patients, and in surviving and deceased patients separately from BL to FU2 as well ($p = 0.066$ and $p = 0.013$).

Table 4.1: Demographic and baseline characteristics.

Characteristics	All (n = 67)	Surviving (n = 49)	Deceased (n = 18)	p-value
Demographic				
Age (years)	57.0 [48.4-66.0]	58.0 [49.0-92.4]	65.5 [57.0-69.8]	0.001
Sex (% female), n (%)	20 (30%)	14 (29%)	6 (33%)	0.706
BMI (kg/m^2)	24.9±3.7	24.7±3.7	25.6±3.4	0.386
BSA (m^2)	1.91 [1.76-2.04]	1.89 [1.76-2.06]	1.94 [1.80-2.02]	0.626
Primary diagnosis, n (%)				0.275
DM (type 2)	7 (10%)	4 (8%)	3 (17%)	
Hypertension	11 (16%)	6 (12%)	5 (28%)	
Glomerulonephritis	16 (24%)	11 (22%)	5 (28%)	
ADPKD	14 (21%)	13 (27%)	1 (6%)	
FSGS	1 (2%)	1 (2%)	0 (0%)	
Other	18 (27%)	14 (29%)	4 (22%)	
Dialysis, n (%)				0.238
Preemptive transplantation, n (%)	21 (31%)	16 (33%)	5 (28%)	
Hemodialysis	27 (40%)	21 (43%)	6 (33%)	
Peritoneal dialysis	12 (18%)	6 (12%)	6 (33%)	
Both	7 (10%)	6 (12%)	1 (6%)	
Duration (months)	30.0 [8.0-45.0]	31.0 [7.0-49.0]	23.5 [11-41.5]	0.635
Arteriovenous fistula	22 (33%)	16 (33%)	6 (33%)	0.958
Renal risk factors, n (%)				
History of CVD	19 (28%)	10 (2%)	9 (50%)	0.017
Hypertension	52 (78%)	38 (78%)	14 (78%)	0.984
Systolic blood pressure (mmHg)	135±16.0	133±15.9	141±14.4	0.080
DM (type II)	10 (15%)	5 (10%)	5 (28%)	0.074
Transplantation, n (%)				
First kidney transplant	64 (96%)	46 (94%)	18 (100%)	0.283
Postmortal donor	31 (46%)	21 (43%)	10 (56%)	0.219
Biochemical measurements				
Tacrolimus (μg/L)	9.1 [6.6-13.6]	10.1 [6.8-14.3]	8.3 [6.6-12.0]	0.489
High sensitive CRP (mg/L)	7.7 [3.1-13.4]	7.5 [3.0-13.5]	7.6 [3.5-13.2]	0.795
Creatinine clearance (mL/min)	42.3±22.8	41.1±22.5	45.8±23.3	0.464
Hematocrit (XX)	0.3±0.0	0.3±0.0	0.3±0.0	0.128
Haemoglobin (mmol/L)	6.9±0.9	7.0±0.9	6.6±0.7	0.088
Virology,n (% igG positive)				
EBV status acceptor	56 (84%)	38 (78%)	18 (100%)	0.028
EBV status donor	36 (54%)	29 (59%)	7 (39%)	0.418
CMV status acceptor	44 (66%)	30 (61%)	14 (78%)	0.206
CMV status donor	44 (66%)	35 (71%)	9 (50%)	0.102

Variables are expressed as mean ±SD or median [IQR]. ADPKD, autosomal dominant polycystic kidney disease; BMI, body mass index; BSA, body surface area; CMV, Cytomegalovirus; CRP, C-reactive protein; CVD, cardiovascular disease; DM, diabetes mellitus; EBV, EpsteinBarr virus; FSGS, focal segmental glomerulosclerosis.

Table 4.2: LV volumetric imaging outcomes of all patients at three time points.

	All	n	Surviving	n	Deceased	n
LVMi (g/m^2)						
BL	36.2 [34.2, 38.3]	66	36.6 [34.2, 39.0]	48	35.3 [31.1, 39.5]	18
FU1	34.6 [32.5, 36.7]	50	34.5 [32.2, 36.8]	38	34.8 [29.1, 40.4]	12
FU2	32.0 [29.5, 34.5] *	38	32.2 [29.7, 34.7] *	30	31.2 [22.3, 40.2]	8
CI (L/min/m^2)						
BL	3.6 [3.4, 3.8]	66	3.6 [3.4, 3.8]	48	3.6 [3.1, 4.0]	18
FU1	3.2 [3.0, 3.5] *	50	3.2 [3.0, 3.4]	38	3.4 [2.6, 4.1]	12
FU2	2.9 [2.7, 3.2] *	38	3.0 [2.7, 3.3] *	30	2.8 [2.4, 3.1] *	8
LVEF (%)						
BL	76.2 [74.4, 78.1]	66	75.4 [73.2, 77.6]	48	78.5 [74.9, 82.1]	18
FU1	77.0 [74.7, 79.3]	50	75.7 [72.9, 78.5]	38	80.9 [77.5, 84.3]	12
FU2	77.6 [75.4, 79.9]	38	76.8 [74.1, 79.4]	30	80.9 [76.4, 85.5]	8
LVEDVi (ml/m^2)						
BL	69.0 [63.6, 74.4]	66	70.6 [64.3, 76.8]	48	64.8 [53.1, 67.5]	18
FU1	65.2 [59.9, 70.4]	50	65.8 [60.3, 71.2]	38	63.3 [48.2, 78.4]	12
FU2	60.9 [56.1, 65.8] *	38	63.2 [57.5, 68.9]	30	52.5 [44.4, 60.6]	8
LVESVi (ml/m^2)						
BL	17.3 [14.7, 19.9]	66	18.4 [15.2, 21.7]	48	14.2 [10.3, 18.0]	18
FU1	15.5 [13.1, 17.8]	50	16.6 [13.7, 19.5]	38	11.9 [8.9, 14.9]	12
FU2	14.1 [11.8, 16.4]	38	15.2 [12.5, 17.9]	30	10.1 [6.9, 13.4]	8
MCF (%)						
BL	61.4 [61.1, 67.2]	66	64.5 [61.1, 67.8]	48	63.3 [55.9, 70.6]	18
FU1	65.3 [61.4, 69.2]	50	65.4 [60.8, 70.0]	38	65.3 [56.8, 73.7]	12
FU2	66.7 [62.4, 70.8]	38	67.3 [62.3, 72.3]	30	64.0 [54.9, 73.2]	8
LVM/EDV						
BL	1.3 [1.2, 1.4]	66	1.3 [1.2, 1.4]	48	1.4 [1.1, 1.7]	18
FU1	1.3 [1.2, 1.4]	50	1.3 [1.2, 1.4]	38	1.4 [1.1, 1.6]	12
FU2	1.3 [1.2, 1.4]	38	1.2 [1.1, 1.3]	30	1.4 [1.1, 1.6]	8

Variables are expressed as mean [95% CI]. CI, cardiac index; LVEDVi, left ventricular end-diastolic volume index; LVEF, left ventricular ejection fraction; LVESVi, left ventricular end-systolic volume index; LVMi, left ventricular mass index; MCF, myocardial contraction fraction. * p-value < 0.05 when compared to baseline.

4.2.2. Strain outcomes of all patients

The mean strain outcomes of all patients at three time points were calculated (Figure 4.2, Table C1). One way ANOVA with repeated measures determined that only the mean GRS differed significantly between time points (p = 0.024). However, post hoc analysis with a Bonferroni adjustment revealed that GRS was not statistically significantly increased (p = 0.063). Strain rates were not significantly different between time points (Table C1).
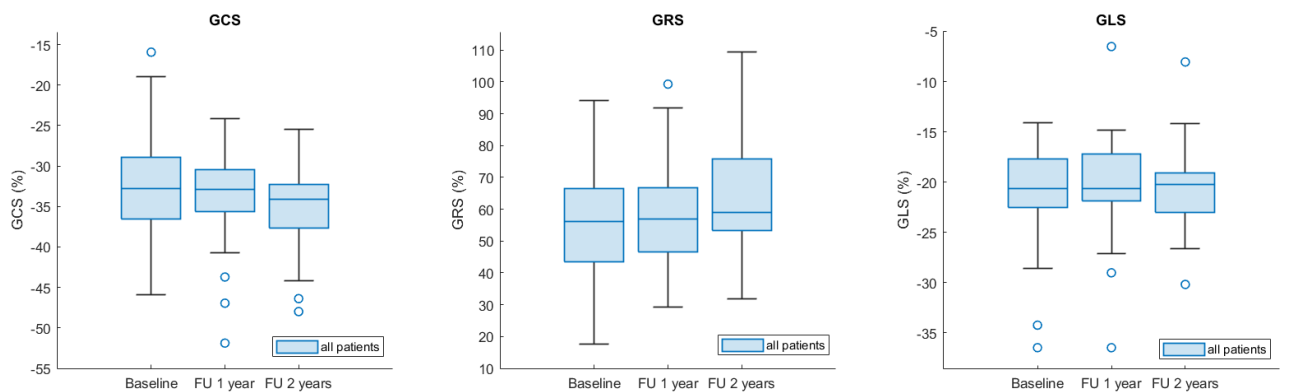
Figure 4.2: Global strain (%) at three time points in circumferential (GCS), radial (GRS) and longitudinal direction (GLS). FU, follow-up.

4.2.3. Strain outcomes of surviving and deceased patients

All strain results of patients, categorized into surviving and deceased, are accessible in Table C2. Global strain results are presented in Figure 4.3. The GRS of surviving patients increased significantly with time ($p = 0.04$). However, post hoc analysis with a Bonferroni adjustment revealed that this improvement was not statistically significant ($p = 0.112$).
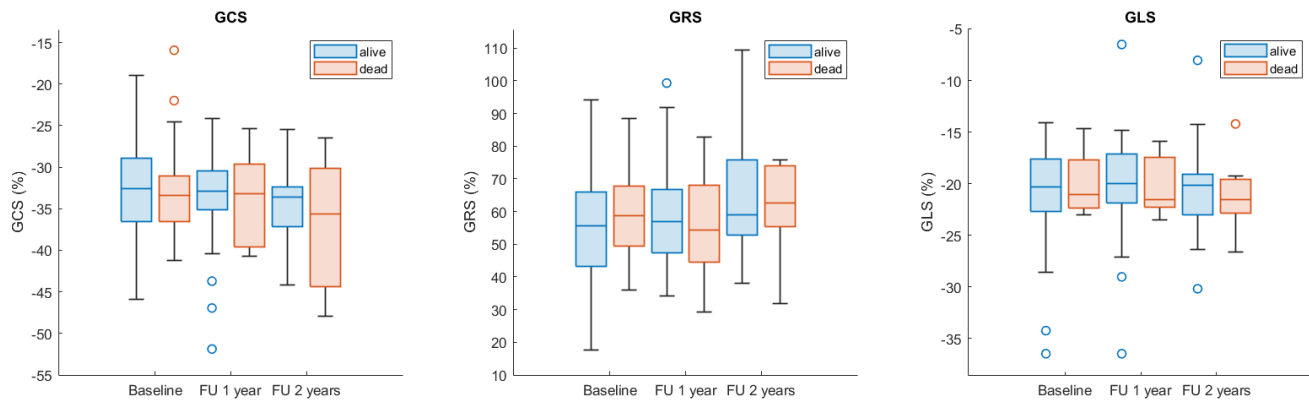
Figure 4.3: Boxplots of global strain (%) grouped by surviving and deceased patients at three time points. FU, follow-up.

When comparing the strain rates of surviving and deceased patients, surviving patients had a significantly higher longitudinal PSSR at two years (-1.0±0.2 versus -1.2±0.4, $p = 0.029$) and longitudinal PEDSR at baseline (1.1±0.5 versus 0.7±0.5, $p = 0.013$) (Figure 4.4, Table C2). Higher absolute values for PSSR and PEDSR values are typically associated with better cardiac function. No other statistically significant differences were found within or between groups.

Figure 4.4: Boxplots of strain rate (1/s) grouped by surviving and deceased patients at three time points. FU, follow-up.

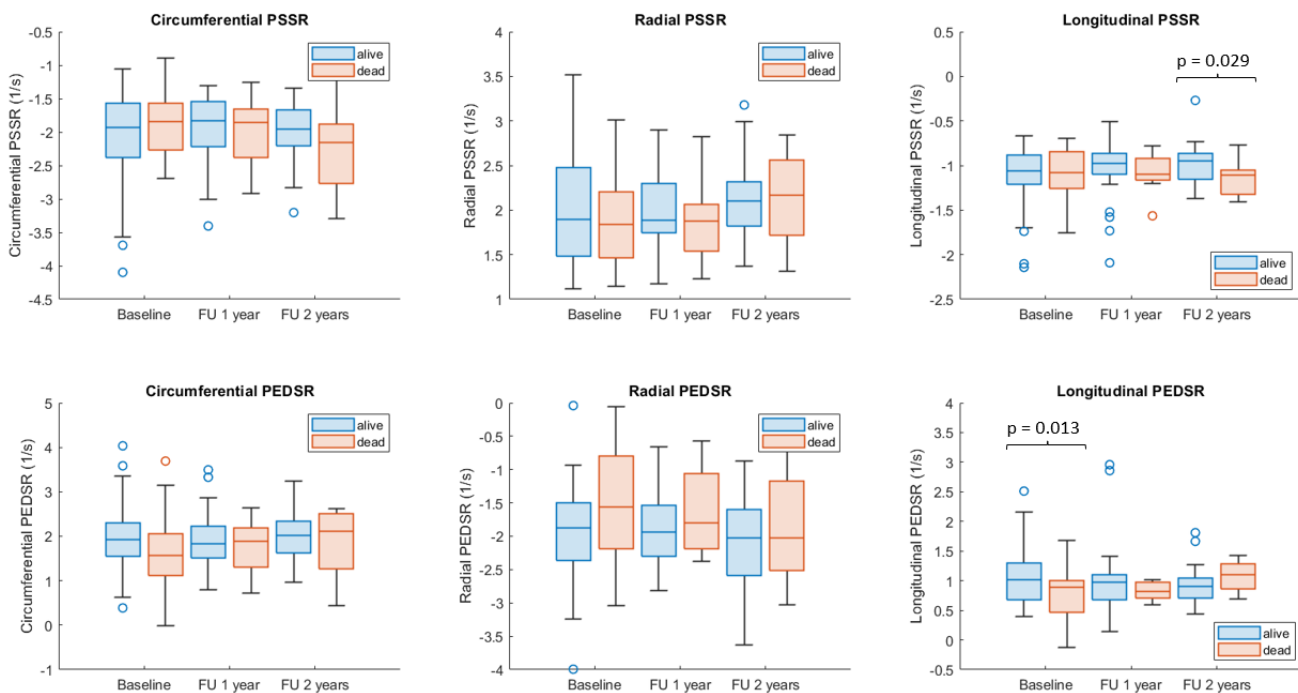A decreased PEDSR in circumferential or longitudinal direction, coupled with an increased PEDSR in radial direction, indicates a decline in the heart's ability to relax during the diastolic phase. This is exemplified by the strain (rate) plots in Figure 4.5 which clearly illustrate the limited presence of diastolic peaks. Although the average changes in PSSR and PEDSR are relatively small both within and between groups, the essential objective remains the early identification of individual patients with diastolic dysfunction.
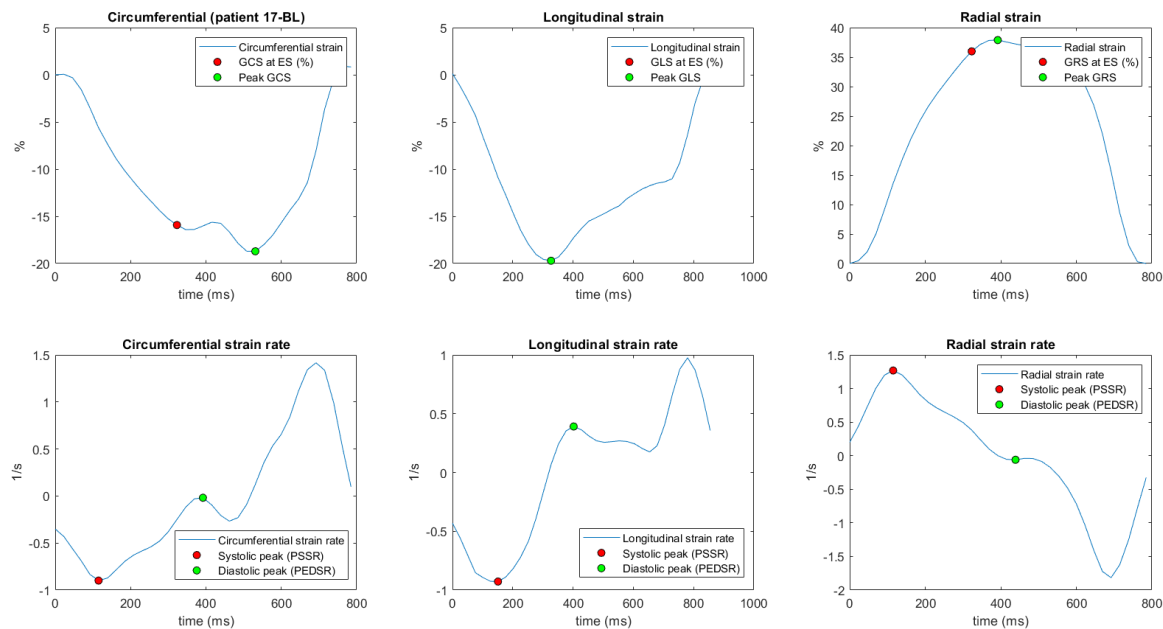

Figure 4.5: Example of strain rate graphs of a patient with low diastolic strain rate peaks, indicating diastolic dysfunction. GCS, global circumferential strain at end-systole (ES); GLS, global longitudinal strain at ES; GRS, global radial strain at ES; PSSR, peak systolic strain rate; PEDSR, peak early diastolic strain rate.

4.3. Predictors of all-cause mortality

This section provides the statistical analysis to identify possible predictors of all-cause mortality of KTx recipients by cardiac MRI. First, optimal cut-off values were determined based on the ROC curve analysis. Subsequently, survival distributions were compared by Kaplan-Meier curves. Finally, to identify independent predictors, a multivariable Cox regression analysis with backward stepwise elimination was employed.

4.3.1. ROC curve analysis

For each imaging outcome, AUC values of the ROC curve were determined to identify differences in survival. At baseline, the volumetric outcomes LVEF, LVEDVi, LVESVi resulted in AUCs > 0.60 (0.633, 0.605 and 0.625). From strain imaging, the PEDSR in circumferential, radial and longitudinal direction resulted in the highest AUCs (0.636, 0,611 and 0,676) (Table 4.3). The ROC curve with the highest AUC, longitudinal PEDSR at baseline, is presented in Figure 4.6.

At FU1, the AUCs of LVEF, LVEDVi and LVESVi increased to 0.698, 0.629 and 0.697, when compared to baseline. Contrastingly, the AUCs of PEDSR in circumferential, radial and longitudinal direction slighty decreased to 0.514, 0.606 and 0.614 (Table C3). At FU2, only volumetric outcomes, including LVEF, CI, LVEDVi, LVESVi and LVM/EDV, resulted in AUC values > 0.60 (Table C4).

From the ROC curves of variables with an AUC > 0.60, the optimal cut-off values were determined (Table 4.3). Additionally, for LVMi the most optimal cutoff was also determined. This was necessary to enable a comparison of the potential usefullness of PEDSR in predicting mortality against LV volumetric outcomes.

Table 4.3: Receiver operating characteristic curve analysis with cutoffs determined
for baseline variables with AUC > 0.600 and the volumetric outcome LVMi.

Variable	AUC	Cut-off	Sensitivity (%)	Specificity (%)	p-value
Volumetric imaging					
LVMi	0.444	34.54	0.611	0.625	0.081
LVEF	0.633	77.74	0.667	0.625	0.052
CI	0.557	-	-	-	-
LVEDVi	0.605	0.500	0.750	56.2	0.077
LVESVi	0.625	0.833	0.617	17.6	0.066
MCF	0.495	-	-	-	-
LVM/EDV	0.582	-	-	-	-
Strain imaging					
GCS	0.460	-	-	-	-
GRS	0.449	-	-	-	-
GLS	0.549	-	-	-	-
cPEDSR	0.636	1.77	0.661	0.596	0.130
rPEDSR	0.611	-1.76	0.556	0.617	0.161
lPEDSR	0.676	1.00	0.833	0.521	0.023
cPSSR	0.546	-	-	-	-
rPSSR	0.556	-	-	-	-
lPSSR	0.512	-	-	-	-

p-values determined from Kaplan-Meier analysis. AUC, area under the curve; CI,
cardiac index; cPEDSR, circumferential peak early diastolic strain rate (PEDSR);
cPSSR, circumferential peak systolic strain rate (PSSR); GCS, global circumferential
strain; GRS, global radial strain; GLS, global longitudinal strain; LVEDVi, left
ventricular end-diastolic volume index; lPEDSR, longitudinal PEDSR; lPSSR,
longitudinal PSSR; LVEF, left ventricular ejection fraction; LVESVi, left ventricular
end-systolic volume index; LVMi, left ventricular mass index; rPEDSR, radial PEDSR;
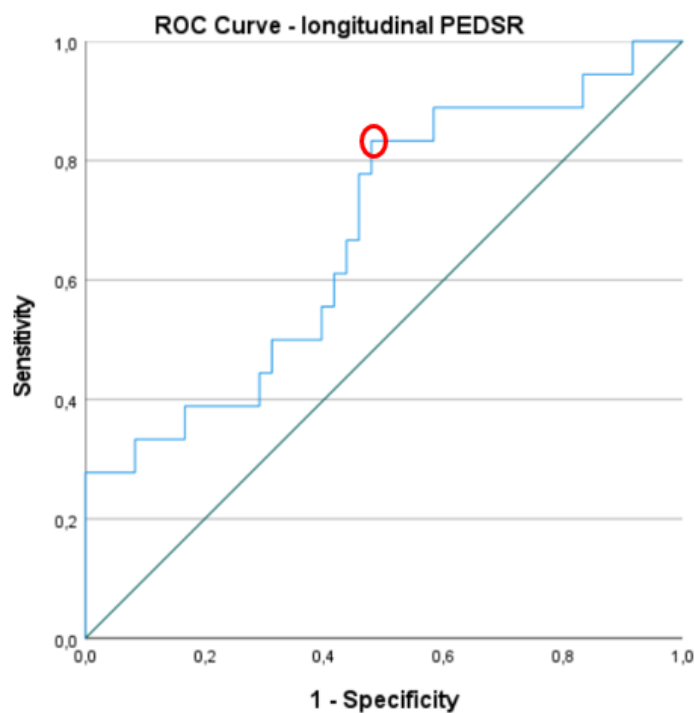rPSSR, radial PSSR.

Figure 4.6: ROC curve based on longitudinal peak early diastolic
strain rate (PEDSR) (1/s) at baseline, with the optimal cutoff
circled in red.

4.3.2. Kaplan-Meier curves

With the optimal cut-off values, a log rank test was run to calculate the corresponding p-values. Regarding LVMi, LVEF, LVM/EDV and radial PEDSR, higher values than the cut-off were linked to all-cause mortality. On the other hand, for CI, LVEDVi, LVESVi, circumferential and longitudinal PEDSR, lower values than the cut-off were connected to all-cause mortality.

At baseline, only significant differences were found based on longitudinal PEDSR with a cutoff value of 1.00 ($\chi2 = 5.163$, p = 0.023) (Figure 4.7). At FU1 the p-value was increased to p = 0.058. At FU1, also significant differences between survival distributions were found based on LVEF, LVEDVi, and LVESVi (p = 0.016, p=0.028 and p=0.023) Table C3. At FU2, this was only LVEDVi with a p-value of 0.037 Table C4. Kaplan-meier curves of variables with the highest AUC at FU1 (LVEF) and FU2 (LVEDVi) are available in Figure C2 and Figure C3.

These findings show that with longitudinal PEDSR it is possible to identify patients at a significant risk of all-cause mortality already at baseline imaging. In contrast, using LV volumetric outcomes, this identification was only achievable starting from FU1.
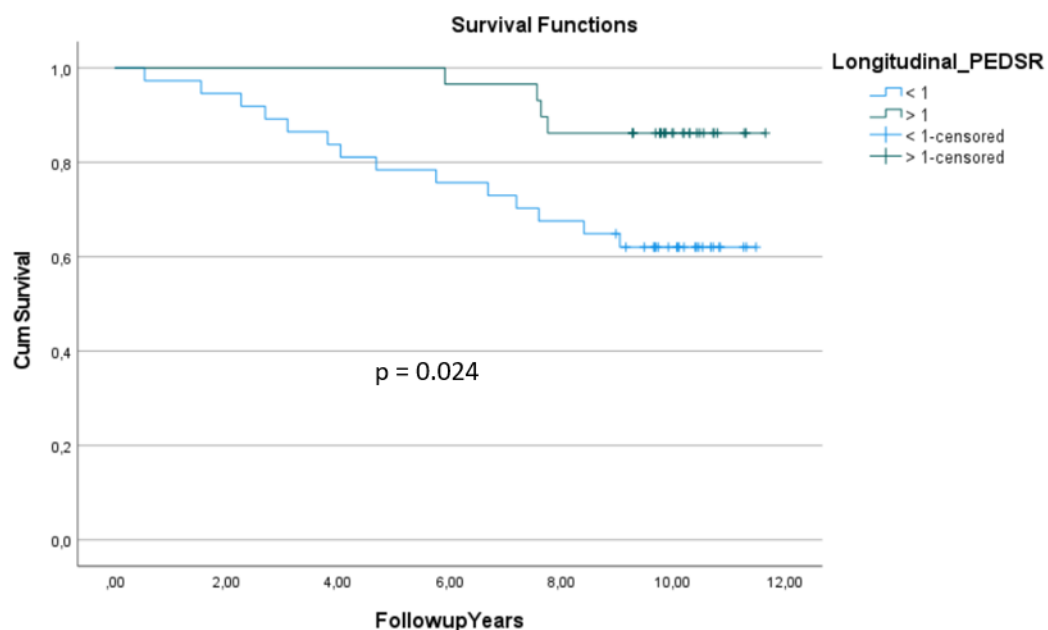
Figure 4.7: Kaplan-Meier survival function based on longitudinal peak early diastolic strain rate (PEDSR) (1/s) at baseline.

4.3.3. Multivariable model

The primary goal was to assess the feasibility of predicting all-cause mortality of KTx recipients by cardiac MRI two weeks post-KTx. For this reason, Cox regression analysis was performed on variables at baseline. In this way, it could be determined whether longitudinal PEDSR < 1.00 at baseline was an independent predictor of survival.

On univariable analysis with each variable entered separately, the variables age, history of CVD, diabetes and PEDSR in three directions showed associations with all-cause mortality with p-values less than 0.2 (Table 4.4). A multivariable model was constructed by combining these variables with the pre-defined clinical characteristics of sex, AV-fistula and dialysis duration. Following backward stepwise elimiation, only the variables sex, age, history of CVD and longitudinal PEDSR were selected in the final model. The inclusion of the variables LVEF, LVEDVi and LVESVi as well led to an unchanged model.

The best independent predictor of all-cause mortality was longitudinal PEDSR < 1.00, with an hazard ratio (HR)) of 3.86 (95% CI 1.19-12.56). Being a female (HR 3.22 [95% CI 1.00-10.36]), having CVD (HR 3.06 [95% CI 1.07-8.75]) and a higher age (HR 1.09 [95% CI 1.02-1.16]) were also linked to an increased risk of all-cause mortality after accounting for other variables. Age and a history of CVD already differed between surviving and deceased patients at baseline (Table 4.1).

Table 4.4: Multivariable model of mortality with longitudinal PEDSR adjusted to univariate clinical and strain rate imaging predictors (at p≤0.20).

Baseline variables	Univariable		Multivariable	
	HR (95% CI)	p-value	HR (95% CI)	p-value
Clinical				
Sex (female)	1.27 (0.48-3.38)	0.634	3.22 (1.00-10.36)	0.050
Age	1.09 (1.03-1.16)	0.004	1.09 (1.02-1.16)	0.009
BMI	1.05 (0.93-1.19)	0.449	-	-
History of CVD	3.03 (1.02-7.64)	0.019	3.06 (1.07-8.75)	0.037
Diabetes	2.72 (0.96-7.68	0.059	-	-
Dialysis duration	0.99 (0.98-1.01)	0.865	-	-
Arteriovenous fistula	1.07 (0.40-2.86)	0.890	-	-
Strain rate imaging				
cPEDSR	2.14 (0.83-5.53)	0.115	-	-
rPEDSR	1.93 (0.76-4.89)	0.167	-	-
lPEDSR	3.37 (1.10-10.24)	0.032	3.86 (1.19-12.56)	0.025

BMI, body mass index; CI, confidence interval; CVD, cardiovascular disease; HR, hazard ratio; cPEDSR, circumferential peak early diastolic strain rate; rPEDSR, radial peak early diastolic strian rate; lPEDSR, longitudinal peak early diastolic strian rate.

In Figure 4.8, patients with and without CVD are stratified by the the longitudinal PEDSR at baseline. It shows that having CVD even more increases the risk of death when the longitudinal PEDSR is below 1.00 ($\chi2 = 11.482$, p = 0.009). The group with PEDSR < 1 and CVD was statistically significant from the group with PEDSR > 1 and no CVD (p<0.001).
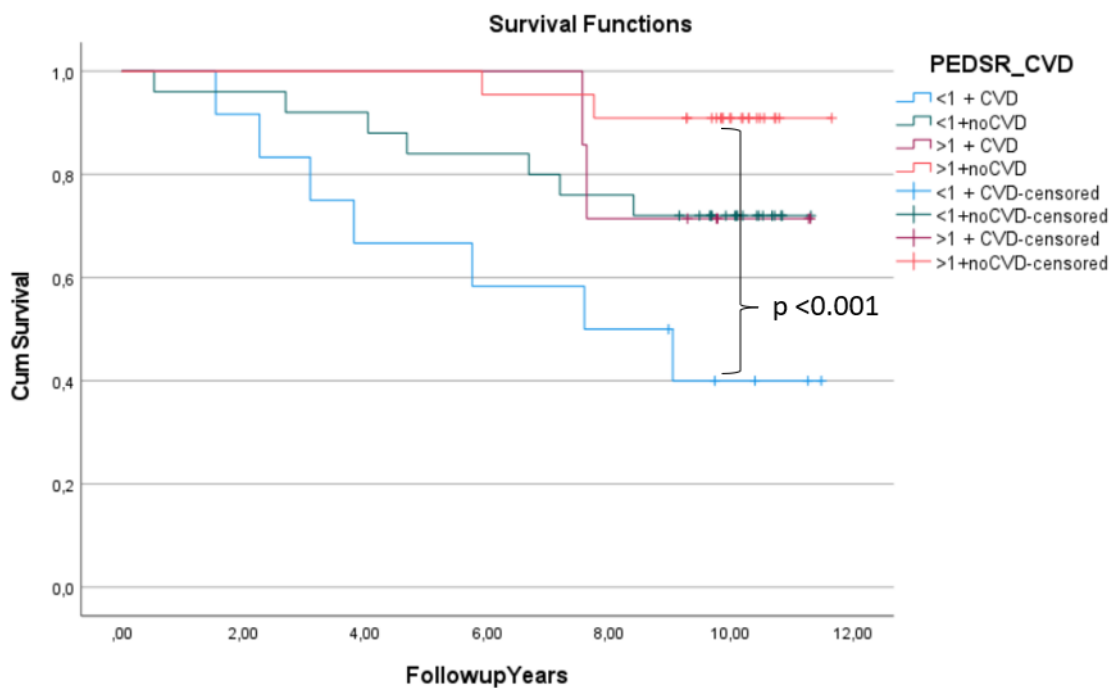
Figure 4.8: Kaplan-Meier survival function based on having longitudinal PEDSR (1/s) < 1 and cardiovascular disease (CVD) at baseline.

4.4. Comparison of ALEGRO groups

Strain results of the three different ALEGRO groups can be found in Appendix B (Table C1. There were no significant differences within or between groups (Table C5, Figure C4, Table C6, Figure C5).

All-cause mortality was 27% over a median follow-up of 10 years. Three patients (15%) had died in the steroid-free group (1), eight (32%) in the standard group (2a) and seven (32%) in the low-dose CNI group (2b). A log rank test determined that the survival distributions between the three groups were not statistically different (Figure 4.9).
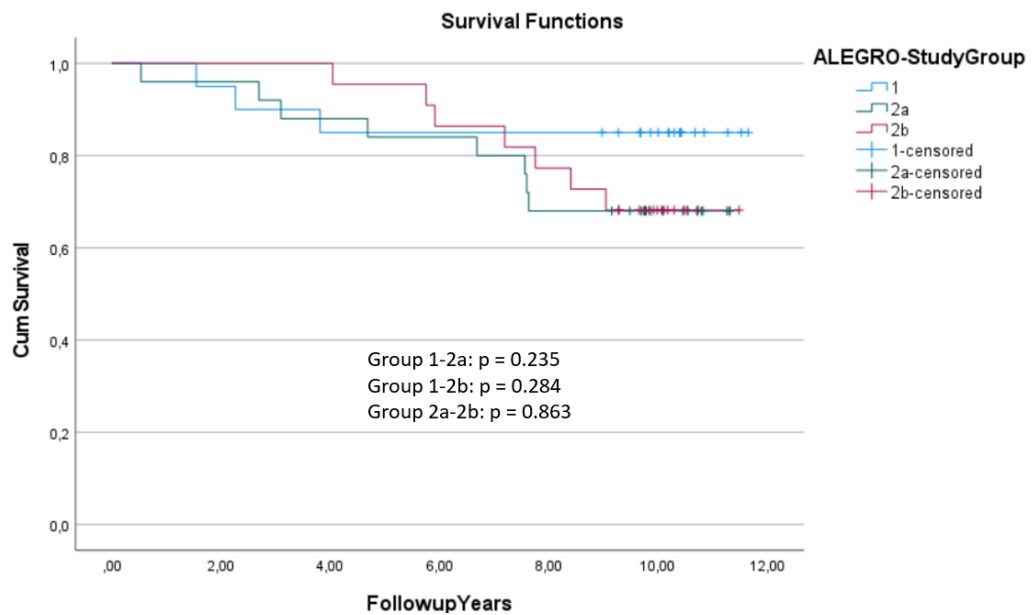
Figure 4.9: Survival distribution of ALEGRO groups. Group 1, steroid-free; Group 2a, standard; Group 2b, low-dose calcineurin inhibitor.

Additionally, there were no significant differences between study groups when adjusted for longitudinal PEDSR (Figure 4.10, Figure 4.11). However, it can be observed that when the longitudinal PEDSR was greater than 1, study group 1 had the highest survival rate.
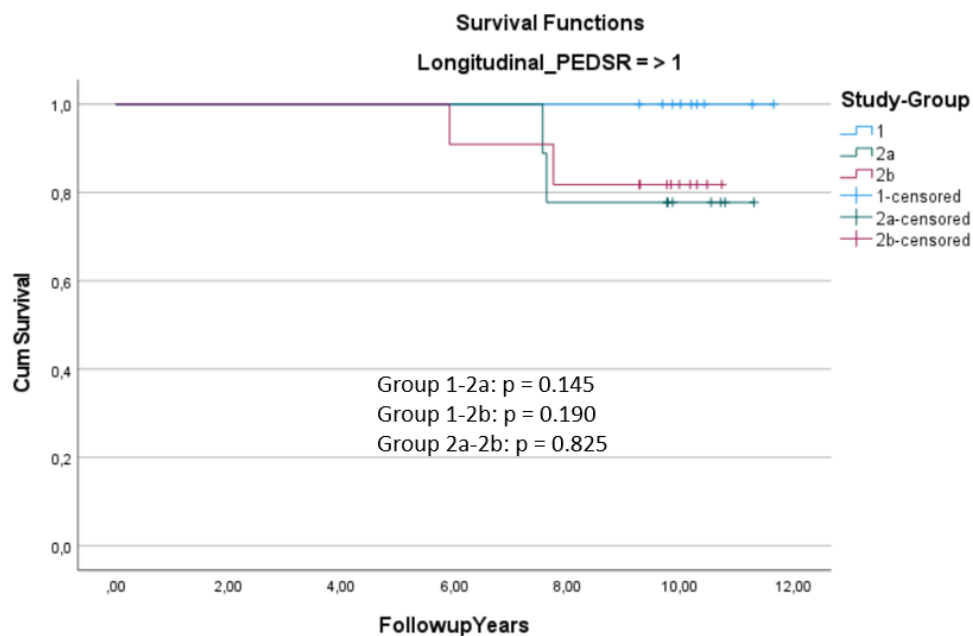
Figure 4.10: Survival distribution of ALEGRO groups with a longitudinal peak early diastolic strain rate (PEDSR) above 1 (1/s). Group 1, steroid-free; Group 2a, standard; Group 2b, low-dose calcineurin inhibitor.
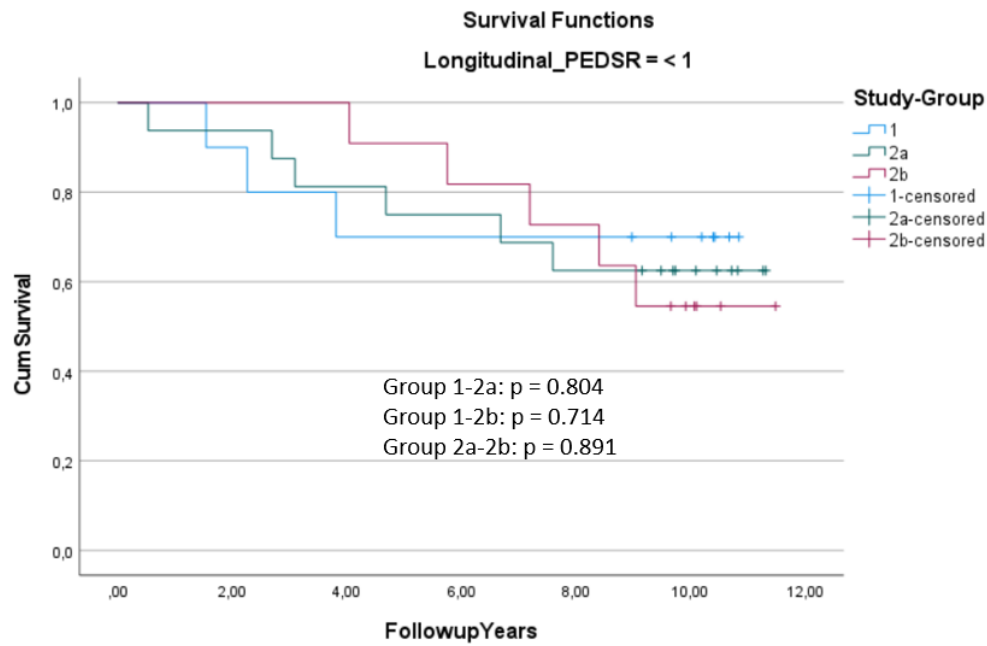
Figure 4.11: Survival distribution of ALEGRO groups with a longitudinal peak early diastolic strain rate (PEDSR) below 1 (1/s). Group 1, steroid-free; Group 2a, standard; Group 2b, low-dose calcineurin inhibitor.

4.5. Intra-observer variability

To analyze the consistency of strain measurements, measurements of fifteen randomly selected scans were repeated. The ICCs of all strain measurements was calculated (Figure 4.12). The ICCs ranged from good to excellent. Specifically, radial strain measurements resulted in lower reproducibility compared to circumferential and longitudinal measurements. The ICC values for ES GRS and peak GRS were classified as good (0.72 and 0.75, respectively), whereas all other measurements were classified as excellent (ranging from 0.79 to 0.99). Interesting to note is that peak global strain values resulted in higher reproducibility compared to values at ES.
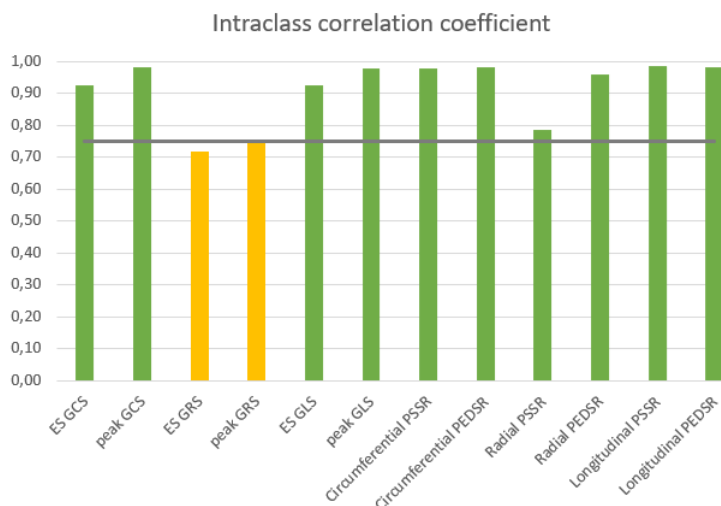
Figure 4.12: Intra-observer variability of strain measurements. ES, end-systolic; GCS, global circumferential strain; GRS, global radial strain; GLS, global longitudinal strain; ICC, intraclass correlation coefficient; PSSR, peak systolic strain rate; PEDSR, peak early diastolic strain rate.

5

Discussion

The findings of this thesis demonstrate that KTx recipients with an increased risk of all-cause mortality can be identified based on diastolic strain rate by cardiac MRI two weeks post-KTx. Longitudinal PEDSR on feature tracking cardiac MRI was independently associated with all-cause mortality during a median follow-up of 10 years. This also applied to the clinical variables age, sex and the presence of CVD at baseline. Incorporating the assessment of longitudinal PEDSR is important for the prognosis of KTx recipients and provides incremental prognostic information beyond clinical and volumetric imaging parameters two weeks post-KTx.

It was hypothesized that myocardial strain has the potential to detect early diastolic dysfunction more effectively when compared to LV volumetric measurements. This was confirmed, as there was no association between LV volumetric imaging outcomes and all-cause mortality at baseline, in contrast to longitudinal PEDSR. With LV volumetric imaging outcomes, an association was only found from FU1. From this, we conclude that with diastolic strain rate, identifying patients with an increased risk of all-cause mortality is possible at a earlier stage compared to LV volumetric imaging outcomes.

5.1. Interpretation of results

The longitudinal PEDSR is not significantly different at FU1 and FU2 anymore. This could be attributed to the regression of myocardial fibrosis post-KTx [1]. However, some variables, including the longitudinal PEDSR at FU2, resulted in AUC values <0.5. This indicates that based on the optimal cut-off value, the model is making predictions that are opposite to the actual outcomes. The classification is poorer than what would be expected by random chance. A possible explanation is that variables with an AUC <0.5 improved more in deceased patients than in surviving patients over time. This could be caused by the reduced sample size at FU1 and FU2. Patients lost to follow-up might have had relatively poor cardiac function. Only scanning the relatively healthy patients may have resulted in an improved mean of the deceased patients at these time points. Changing the test direction would have led to AUC values >0.5. However, this would lead to a prediction with no practical value. For this reason, the ROC curve's test direction was established based on the baseline variables relative to normal ranges and maintained consistently.

For longitudinal PEDSR, a lower limit of normality of 1 s^1 was determined, which is similar to the study of Morris et al. [29]. However, the longitudinal PEDSR is significantly higher in women compared to men [29, 30]. As a result, if women have a longitudinal PEDSR below 1 s^1, their value is notably lower than what is considered normal. This explains why being female was independently associated with a higher risk of all-cause mortality.

The reason why only PEDSR in longitudinal direction was independently associated may be because relaxation of the heart mainly lengthens along the longitudinal axis. In contrast, in a previous study by Kramann et al., circumferential and radial strain parameters were independent risk factors for cardiovascular and all-cause mortality in ESKD patients [8]. However, these results were based on echocardiographic strain measured in only six mid-segments, and the follow-up time of 2.5 years was

much shorter than in this thesis. Additionally, the previously conducted meta-analysis showed that circumferential and radial strain improve post-KTx, and may therefore not be suitable for predicting long-term survival.

The GLS was not associated with all-cause mortality, in contrast to studies in patients with heart failure and preserved ejection fraction [1, 31]. This may be due to the fact that GLS is a marker of systolic function. However, the prognosis of included KTx recipients was primarily related to diastolic dysfunction.

For MCF and LVM/EDV, no differences between time points or study groups were found, and both were not associated with all-cause mortality. An impaired MCF is more an indication of systolic dysfunction [32], which may not be relevant to KTx recipients. The LVM/EDV was shown to be associated with diastolic function in earlier studies [22, 23]. However, this thesis indicates that LVM/EDV is also not an effective measure for identifying patients with a high risk of mortality.

Additionally, differences between the three immunosuppression groups of the ALEGRO study were analyzed. Immunosuppression after KTx is necessary to prevent acute graft rejection. However, it is also known to be a major cause of the metabolic syndrome, which is in turn associated with the high cardiovascular mortality after KTx [33, 34]. In the interim analysis of the ALEGRO study at six months, it was shown that early steroid withdrawal (group 1) was associated with a more favourable cardiovascular risk profile [35]. In the study of Mourer et al., CNI withdrawal (similar to group 2b) prevented deterioration of LV diastolic function [36]. However, in this thesis, no significant differences in strain outcomes and all-cause mortality were found. Unfortunately, it was not possible to examine effects on cardiovascular mortality or SAEs, as data from patients' electronic medical records were insufficient to allow reliable examination. It is important to include these outcomes before the noninferiority of the interventional immunosuppressive regimen in the ALEGRO study can be confirmed.

A number of factors influencing strain results must be taken into account. First, variations in strain results can be caused by the used modality and software [19, 37]. The use of feature tracking cardiac MRI is the preferred method for strain analysis. Cardiac MRI is the gold standard for the assessment of cardiac structure and function in ESKD patients [14, 38], and feature tracking enables fast and retrospective strain analysis on routinely acquired cine imaging [1]. However, strain assessment by different feature tracking software packages is not interchangeable. Pérez et al. also shows the relatively low reproducibility of GRS by Medis, similar to our findings [39]. Secondly, the field strengths must be taken into consideration as both 1.5T and 3T imaging were used. Minimal bias was seen in a previous study by Ayton et al. In particular, an ICC of 0.69 was obtained with QStrain for longitudinal PEDSR [40]. These findings emphasize the importance of taking into account all study characteristics when comparing absolute strain values.

5.2. Future recommendations

Several additional analyses can supplement those included in this thesis. First, it is interesting to evaluate if the association between longitudinal PEDSR and all-cause mortality is also identifiable already pre-KTx. If this is indeed the case, the assessment of longitudinal strain rate by cardiac MRI could be added to the pre-transplant evaluation. For example, the TRANSFORM study could be used as patients underwent cardiac MRI one week pre-KTx (for living donations only). Cardiovascular morbidity and mortality were similar between different immunosuppressive groups. However, the predictive value of strain was not assessed [41]. Secondly, it may be relevant to determine the importance of other variables related to diastolic function in predicting mortality. Examples are the E/A ratio (ratio of PEDSR to PLDSR), E/e' ratio (ratio of PEDSR to early diastolic mitral annular velocity), deceleration time (DT) of the PEDSR peak and isovolumetric relaxation time (IVRT) [42]. Additionally, the direct assessment of fibrosis may be relevant as higher baseline levels of fibrosis were associated with a higher loss of longitudinal PEDSR over one year in ESKD patients [43]. The direct assessment of myocardial fibrosis requires T1 mapping or contrast-enhanced imaging. However, the absolute difference between the global peak and ES strain can possibly be used for this as this indicates post-systolic shortening of the systole. This, in turn, might also be related to myocardial fibrosis, causing delayed or prolonged shortening. Finally, the assessment of epicardial adipose tissue might be interesting as this is shown to be an independent risk factor of diastolic dysfunction [44].

Besides the importance of early identification of KTx recipients with a high risk of mortality, it is important to investigate in cardiovascular therapeutics for these patients. In this way, irreversible myocardial fibrosis can be minimized. Treatments with antifibrotic properties have been studied before in ESKD patients, like mineralocorticoid receptor antagonists, however, their effect on myocardial strain was not assessed [1]. Further, patients with a low eGFR, prevalent in ESKD and KTx recipients, are often excluded from trials. This addresses the importance of the now ongoing renal lifecycle trial, which examines the effect of a sodium glucose co-transporter 2 (SGLT2) inhibitor [45]. The effect will also be evaluated by cardiac MRI in participants with advanced chronic kidney disease. However, more large-scale studies will be required to assess the effect of cardiovascular therapeutics on the overall prognosis of KTx recipients [46].

5.3. Conclusion

In conclusion, diastolic strain rate by cardiac MRI two weeks post-KTx can be used for the early identification of KTx recipients with an increased risk of all-cause mortality. Longitudinal PEDSR independently predicted all-cause mortality during a median follow-up of 10 years, in contrast to LV volumetric outcomes. There were no differences in survival between immunosuppression groups. Further research in cardiovascular therapeutics is an essential next step in improving the prognosis of KTx recipients.

Bibliography

[1]   Alastair J. Rankin et al. "Global longitudinal strain by feature-tracking cardiovascular magnetic resonance imaging predicts mortality in patients with end-stage kidney disease". In: Clinical Kidney Journal 14.10 (Oct. 2021), pp. 2187–2196. DOI: 10.1093/ckj/sfab020.

[2]   Paul A. Devine, Aisling E. Courtney, and Alexander P. Maxwell. Cardiovascular risk in renal transplant recipients. June 2019. DOI: 10.1007/s40620-018-0549-4.

[3]   Nicola C Edwards et al. Defining the Natural History of Uremic Cardiomyopathy in Chronic Kidney Disease The Role of Cardiovascular Magnetic Resonance. Tech. rep. 2014.

[4]   Kan Zhang et al. "A Comparison of Global Longitudinal, Circumferential, and Radial Strain to Predict Outcomes After Cardiac Surgery". In: Journal of Cardiothoracic and Vascular Anesthesia 33.5 (May 2019), pp. 1315–1322. DOI: 10.1053/j.jvca.2018.10.031.

[5]   D M Sobh et al. "Left Ventricular Strain Analysis by Tissue Tracking- Cardiac Magnetic Resonance for early detection of Cardiac Dysfunction in children with End-Stage Renal Disease". eng. In: J Magn Reson Imaging 54.5 (2021), pp. 1476–1485. DOI: 10.1002/jmri.27700.

[6]   Kartheek Garikapati et al. Uraemic Cardiomyopathy: A Review of Current Literature. 2021. DOI: 10.1177/1179546821998347.

[7]   Xiaoliang Wang and Joseph I. Shapiro. Evolving concepts in the pathogenesis of uraemic cardiomyopathy. Mar. 2019. DOI: 10.1038/s41581-018-0101-8.

[8]   Rafael Kramann et al. "Speckle tracking echocardiography detects uremic cardiomyopathy early and predicts cardiovascular mortality in ESRD". In: Journal of the American Society of Nephrology 25.10 (Oct. 2014), pp. 2351–2365. DOI: 10.1681/ASN.2013070734.

[9]   Jiun Chi Huang et al. "Ratio of early mitral inflow velocity to the global diastolic strain rate and global left ventricular longitudinal systolic strain predict overall mortality and major adverse cardiovascular events in hemodialysis patients". In: Disease Markers 2019 (2019). DOI: 10.1155/2019/7512805.

[10]   Tao Zhang, Jing Li, and Shili Cao. "Prognostic value of left ventricular global longitudinal strain in chronic kidney disease patients: a systematic review and meta-analysis". In: International Urology and Nephrology 52.9 (Sept. 2020), pp. 1747–1756. DOI: 10.1007/s11255-020-02492-0.

[11]   Laura Jahn et al. "Speckle Tracking Echocardiography and All-Cause and Cardiovascular Mortality Risk in Chronic Kidney Disease Patients". In: Kidney and Blood Pressure Research 44.4 (Aug. 2019), pp. 690–703. DOI: 10.1159/000501225.

[12]   Nicholas S. Burris et al. "Feature Tracking Cardiac MRI Reveals Abnormalities in Ventricular Function in Patients With Bicuspid Aortic Valve and Preserved Ejection Fraction". In: Tomography (Ann Arbor, Mich.) 4.1 (Mar. 2018), pp. 26–32. DOI: 10.18383/j.tom.2018.00005.

[13]   B Schaefer et al. "Cardiac magnetic resonance imaging in children with chronic kidney disease and renal transplantation". eng. In: Pediatr Transplant 16.4 (2012), pp. 350–356. DOI: 10.1111/j.1399-3046.2012.01672.x.

[14]   L C Pickup et al. "Changes in left ventricular structure and function associated with renal transplantation: a systematic review and meta-analysis". eng. In: ESC Heart Fail 8.3 (2021), pp. 2045–2057. DOI: 10.1002/ehf2.13283.

[15]   Manuel D. Cerqueira et al. "Standardized Myocardial Segmentation and Nomenclature for Tomographic Imaging of the Heart". In: Circulation 105.4 (Jan. 2002), pp. 539–542. DOI: 10.1161/hc0402.102975.

[16]   A. Scatteia, A. Baritussio, and C. Bucciarelli-Ducci. Strain imaging using cardiac magnetic resonance. July 2017. DOI: 10.1007/s10741-017-9621-8.

[17]   Han Li et al. "Heart failure with preserved ejection fraction in post myocardial infarction patients: a myocardial magnetic resonance (MR) tissue tracking study". In: Quantitative Imaging in Medicine and Surgery 13.3 (Mar. 2023), pp. 1721–1739. DOI: 10.21037/qims-22-793.

[18]   Gianni Pedrizzetti et al. Principles of cardiovascular magnetic resonance feature tracking and echocardiographic speckle tracking for informed clinical use. Aug. 2016. DOI: 10.1186/s12968-016-0269-7.

[19] M. S. Amzulescu et al. Myocardial strain imaging: Review of general principles, validation, and sources of discrepancies. June 2019. DOI: 10.1093/ehjci/jez041.

[20] Qian Tao et al. "Deep learning-based method for fully automatic quantification of left ventricle function from cine MR images: A multivendor, multicenter study". In: Radiology 290.1 (Jan. 2019), pp. 81–88. DOI: 10.1148/radiol.2018180513.

[21] Inna Y. Gong et al. "Cardiovascular magnetic resonance left ventricular strain in end-stage renal disease patients after kidney transplantation". In: Journal of Cardiovascular Magnetic Resonance 20.1 (Dec. 2018). DOI: 10.1186/s12968-018-0504-5.

[22] Maria Lembo et al. "Impact of left ventricular mass/end-diastolic volume ratio by three-dimensional echocardiography on two-dimensional global longitudinal strain and diastolic function in native hypertensive patients". In: Journal of Hypertension 37.10 (Oct. 2019), pp. 2041–2047. DOI: 10.1097/HJH.0000000000002147.

[23] Hildo J. Lamb et al. "Left ventricular remodeling early after aortic valve replacement: Differential effects on diastolic function in aortic valve stenosis and aortic regurgitation". In: Journal of the American College of Cardiology 40.12 (Dec. 2002), pp. 2182–2188. DOI: 10.1016/S0735-1097(02)02604-9.

[24] Yuichi J. Shimada et al. "Myocardial Contraction Fraction Predicts Cardiovascular Events in Patients With Hypertrophic Cardiomyopathy and Normal Ejection Fraction". In: Journal of Cardiac Failure 25.6 (June 2019), pp. 450–456. DOI: 10.1016/j.cardfail.2019.03.016.

[25] Myocardial contraction fraction: an underused imaging biomarker. Tech. rep.

[26] Jens Uwe Voigt et al. "Definitions for a common standard for 2D speckle tracking echocardiography: consensus document of the EACVI/ASE/Industry Task Force to standardize deformation imaging". In: European heart journal cardiovascular Imaging 16.1 (Jan. 2015), pp. 1–11. DOI: 10.1093/ehjci/jeu184.

[27] Domenic V. Cicchetti. "Guidelines, criteria, and rules of thumb for evaluating normed and standardized assessment instruments in psychology." In: Psychological Assessment 6.4 (Dec. 1994), pp. 284–290. DOI: 10.1037/1040-3590.6.4.284.

[28] C. Cuspidi et al. "Indexation of left ventricular mass to body surface area and height to allometric power of 2.7: Is the difference limited to obese hypertensives?" In: Journal of Human Hypertension 23.11 (2009), pp. 728–734. DOI: 10.1038/jhh.2009.16.

[29] Daniel A. Morris et al. "Lower limit of normality and clinical relevance of left ventricular early diastolic strain rate for the detection of left ventricular diastolic dysfunction". In: European Heart Journal Cardiovascular Imaging 19.8 (Aug. 2018), pp. 905–915. DOI: 10.1093/ehjci/jex185.

[30] R. W.J. van Grootel et al. "Influence of age and sex on left ventricular diastolic strain analysis". In: International Journal of Cardiovascular Imaging 35.3 (Mar. 2019), pp. 491–498. DOI: 10.1007/s10554-018-1480-4.

[31] Simone Romano et al. "Feature-Tracking Global Longitudinal Strain Predicts Mortality in Patients With Preserved Ejection Fraction: A Multicenter Study". In: JACC: Cardiovascular Imaging 13.4 (Apr. 2020), pp. 940–947. DOI: 10.1016/j.jcmg.2019.10.004.

[32] Dan Rusinaru et al. "Myocardial Contraction Fraction for Risk Stratification in Low-Gradient Aortic Stenosis with Preserved Ejection Fraction". In: Circulation: Cardiovascular Imaging 14.8 (Aug. 2021), E012257. DOI: 10.1161/CIRCIMAGING.120.012257.

[33] Aiko P.J. De Vries et al. "Fatty kidney: emerging role of ectopic lipid in obesity-related renal disease". In: The Lancet Diabetes & Endocrinology 2.5 (May 2014), pp. 417–426. DOI: 10.1016/S2213-8587(14)70065-8.

[34] Aiko P.J. De Vries et al. "Metabolic syndrome is associated with impaired long-term renal allograft function; not all component criteria contribute equally". In: American Journal of Transplantation 4.10 (Oct. 2004), pp. 1675–1683. DOI: 10.1111/j.1600-6143.2004.00558.x.

[35] Marit S. Van Sandwijk et al. "Early steroid withdrawal compared with standard immunosuppression in kidney transplantation - Interim analysis of the Amsterdam-Leiden-Groningen randomized controlled trial". In: Transplantation Direct 4.6 (June 2018). DOI: 10.1097/TXD.0000000000000794.

[36] Jacqueline S. Mourer et al. "Late calcineurin inhibitor withdrawal prevents progressive left ventricular diastolic dysfunction in renal transplant recipients". In: Transplantation 94.7 (Oct. 2012), pp. 721–728. DOI: 10.1097/TP.0b013e3182603297.

[37] Zahra Raisi-Estabragh et al. Variation in left ventricular cardiac magnetic resonance normal reference ranges: systematic review and meta-analysis. May 2021. DOI: 10.1093/ehjci/jeaa089.

[38]   F Schaefer et al. "Cardiovascular Phenotypes in Children with CKD: The 4C Study". eng. In: Clin J Am
        Soc Nephrol 12.1 (2017), pp. 19–28. DOI: 10.2215/cjn.01090216.

[39]   Manuel Barreiro-Pérez et al. "Left ventricular global myocardial strain assessment comparing the repro-
        ducibility of four commercially available CMR-feature tracking algorithms". In: European Radiology 28.12
        (Dec. 2018), pp. 5137–5147. DOI: 10.1007/s00330-018-5538-4.

[40]   Sarah L. Ayton et al. "The Interfield Strength Agreement of Left Ventricular Strain Measurements at
        1.5ăT and 3ăT Using Cardiac MRI Feature Tracking". In: Journal of Magnetic Resonance Imaging 57.4
        (Apr. 2023), pp. 1250–1261. DOI: 10.1002/jmri.28328.

[41]   Claudia Sommerer et al. "Cardiovascular Outcomes in De Novo Kidney Transplant Recipients Receiving
        Everolimus and Reduced Calcineurin Inhibitor or Standard Triple Therapy: 24-month Post Hoc Analysis
        From TRANSFORM Study". In: Transplantation 107.7 (July 2023), pp. 1593–1604. DOI: 10.1097/tp.
        0000000000004555.

[42]   Jos J.M. Westenberg. CMR for Assessment of Diastolic Function. Apr. 2011. DOI: 10.1007/s12410-
        011-9070-z.

[43]   T A Stromp et al. "Quantitative Gadolinium-Free Cardiac Fibrosis Imaging in End Stage Renal Disease
        Patients Reveals A Longitudinal Correlation with Structural and Functional Decline". eng. In: Sci Rep
        8.1 (2018), p. 16972. DOI: 10.1038/s41598-018-35394-4.

[44]   H Zhou et al. "Magnetic Resonance Imaging Quantification of Accumulation of Epicardial Adipose Tissue
        Adds Independent Risks for Diastolic Dysfunction among Dialysis Patients". eng. In: J Magn Reson
        Imaging 56.4 (2022), pp. 1184–1194. DOI: 10.1002/jmri.28081.

[45]   The RENAL LIFECYCLE Trial: A RCT to Assess the Effect of Dapagliflozin on Renal and Cardiovascular
        Outcomes in Patients With Severe CKD. July 2023.

[46]   Jonathan C.L. Rodrigues et al. "Comprehensive characterisation of hypertensive heart disease left ven-
        tricular phenotypes". In: Heart 102.20 (Oct. 2016), pp. 1671–1679. DOI: 10.1136/heartjnl-2016-
        309576.

<div align="right">

A

</div>
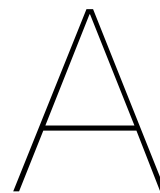
ALEGRO trial

Detailed information about the ALEGRO trial's protocol is outlined in the following sections. It starts with the rationale and study objectives. Hereafter, the in- and exclusion criteria, as well as the different randomization groups are presented. Lastly, results of the interim analysis at 6-months are shortly discussed.

Rationale

Quadruple immunosuppression consisting of an induction treatment, followed by mycophenolate mofetil (MMF), a calcineurin inhibitor (CNI) and steroids results in low rejection rates and excellent graft survival post-KTx. Despite this success, mortality and morbidity in transplant recipients is relatively high due to side effects of immunosuppressive strategies. The incidence of hypertension, hypercholesterolemia and diabetes mellitus is relatively high. This is one of the reasons for the high cardiovascular mortality in renal transplant recipients. A potential cause is the use of steroids and CNIs. CNIs may play an important role in the development of chronic allograft nephropathy causing poor kidney function and cardiovascular disease. However differences between CNIs are shown with regard to the incidence of these side effects and graft function. Also infections and malignancies are the result of immunosuppression in general. In some countries malignancies are the most frequent cause of death in kidney transplant recipients. Steroids play an important role in the development of osteoporosis in renal transplant recipients.

Objectives

The ALEGRO trial was a prospective, open randomized multicenter study, in which it was aimed to achieve optimal immune suppression and optimal reduction of severe side effects, especially reduction of drug induced damage to the vasculature of heart and kidney. Immunosuppression without steroids and CNI minimization was compared to standard immunosuppression, consisting of tacrolimus once daily (OD), MMF and corticosteroids.

Primary endpoint was renal function, proteinuria and microalbuminuria measured 3, 12, and 24 months after transplantation. Secondary endpoints were the degree of tubular atrophy and interstitial fibrosis and the degree of arteriolar hyalinosis in renal biopsies taken at 12 and 24 months after transplantation. Other secondary endpoints were patient and graft survival, the incidence of allograft rejection, cardiovascular accidents, (no contrast) MRI-assessed vascular function (aortic pulse wave velocity), heart function and dimensions, and body fat distribution; blood pressure, the number of anti-hypertensives, lipid profile, the incidence of malignancies, the incidence of infectious complications, the incidence of post transplant diabetes mellitus and the development of osteoporosis.

In- and exclusion criteria

Patients who will receive their first or second renal transplant will be eligible for this study.

Inclusion criteria:

1. Female or male, aged between 18 and 80 years.

2. Recipient of a kidney graft (first or second) from a deceased (heartbeating or non-heartbeating) donor or living (non-human leukocyte antigen (HLA) identical) donor.

3. The patient understands the purpose and risks of the study and has given written informed consent to participate in the study.

Exclusion criteria:

1. Patients with multi-organ transplants.

2. Patients who are receiving a third or fourth transplant.

3. Patients who have >75% (current or historic) panel reactive antibodies.

4. Patients receiving a kidney from a HLA identical donor

5. Female patients who are pregnant or unwilling to use adequate contraception during the study

6. Patients with contra-indications for MRI will still be eligible for inclusion in the study, but will be excluded from MRI measurements for the respective secondary endpoints.

Eligible patients underwent cardiac MRI. No contrast was involved to acquire the images. Patients with contraindications for MRI measurement were excluded from assessment. The following contra-indications applied:

1. Metal containing materials in or on the body (piercings, braces, pacemakers, metal clips, insulin pumps, etc. according to local MRI protocol)

2. Claustrophobia

3. Patients who have >75% (current or historic) panel reactive antibodies.

4. Incapacity to lie flat for more than 30 minutes (e.g. orthopnea).

Randomization groups

Before transplantation patients were randomized 1:1:1 in three groups (Figure A1). 300 patients were necessary for between-group comparisons; which implies 100 patients in each treatment arm. Group 1 was treated with basiliximab induction and a three day course of steroids (prednisolone) followed by a steroid free maintenance regimen consisting of standard-dose tacrolimus OD and MMF. Group 2 was treated with basiliximab induction followed by standard-dose tacrolimus OD, MMF and steroids. Group 3 was treated with basiliximab induction followed by standard-dose tacrolimus OD for six months, whereafter the dose will be reduced plus MMF and steroids.
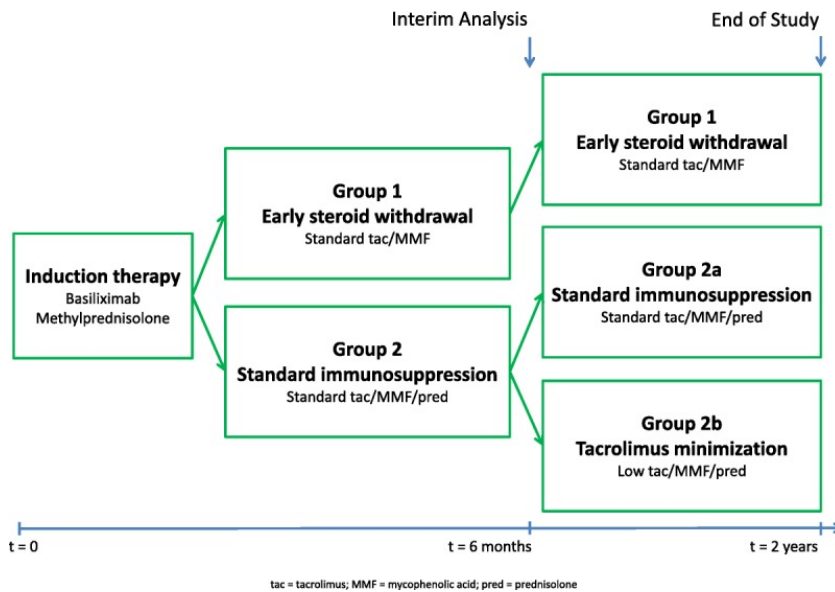
Figure A1: Schematic overview of the ALEGRO trial.

References

1. J.S.F. Sanders (2012, March 22 - 2022, January 11) Steroid Free Immunosuppression or Calcineurin Inhibitor Minimization After Basiliximab Induction Therapy in Kidney Transplantation: Comparison With a Standard Quadruple Immunosuppressive Regimen (Allegro). Identifier NCT01560572. https://classic.clinicaltrials.gov/ct2/show/NCT01560572

2. J.S.F. Sanders (2011, August 26) Amsterdam LEiden GROningen (ALLEGRO): Steroid free immunosuppression or calcineurin inhibitor minimization after Basiliximab induction therapy in kidney transplantation: Comparison with a standard quadruple immunosuppressive regimen. Clinical study protocol (Version: December 2010).

3. M.S. Van Sandwijk et al. Early Steroid Withdrawal Compared With Standard Immunosuppression in Kidney Transplantation - Interim Analysis of the Amsterdam-Leiden-Groningen Randomized Controlled Trial. Transplantation direct, 4(6), e354.
https://doi.org/10.1097/TXD.0000000000000794.

B

Supplementary Information

Comparison of peak and end-systolic strain

The LV global strain was assessed both at the maximum/minimum (peak) and the ES phase. The means of all patients at baseline were compared (Figure C1). For circumferential and longitudinal strain, the peak values resulted in lower values compared to the ES phase (-34.41±6.3 versus -32.81±6.1 and -21.63±4.3 versus -20.73±4.1). The peak radial strain was higher compared to values at ES (58.6±15.7 versus 56.2±16.0). The maximum absolute difference within a patient was 6.3, 5.1 and 9.9 for circumferential, longitudinal and radial strain, respectively.
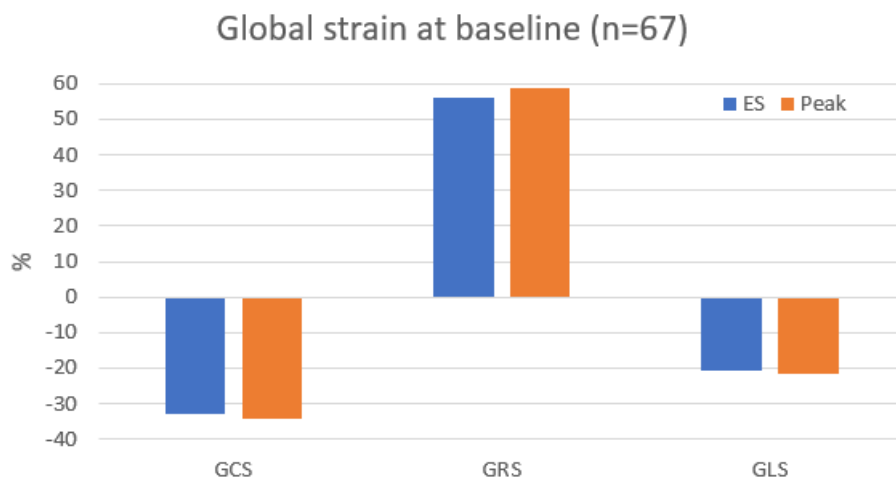

Figure C1: Comparison of peak global strain and at end-systole (ES). GCS, global circumferential strain; GRS, global radial strain; GLS, global longitudinal strain.

Strain outcomes of all and surviving/deceased patients

Table C1: Strain outcomes of all patients at baseline (n=67), follow-up at 1 year (n=50) and 2 years (n=38).

	Circumferential	n	Radial	n	Longitudinal	n
Global						
BL	-32.8 [-34.3, -31.3]	65	56.3 [52.3, 60.3]	65	-20.7 [-21.7, -19.7]	67
FU1	-33.7 [-35.2, -32.1]	48	57.9 [53.6, 62.1]	48	-20.0 [-21.2, -18.8]	50
FU2	-35.0 [-36.7, -33.3]	38	64.2 [58.2, 70.1]	38	-20.5 [-21.8, -19.1]	38
PSSR						
BL	-2.0 [-2.2, -1.8]	65	2.0 [1.8, 2.1]	65	-1.1 [-1.2, -1.0]	67
FU1	-2.0 [-2.1, -1.8]	48	1.9 [1.8, 2.1]	48	-1.0 [-1.1, -1.0]	50
FU2	-2.1 [-2.2, -1.9]	38	2.1 [2.0, 2.3]	38	-1.0 [-1.1, -1.0]	38
PEDSR						
BL	1.9 [1.7, 2.1]	65	-1.8 [-2.0, -1.6]	65	1.0 [0.8, 1.1]	66
FU1	1.8 [1.6, 2.0]	48	-1.8 [-2.0, -1.7]	48	0.9 [0.8, 1.1]	50
FU2	2.0 [1.8, 2.2]	38	-2.0 [-2.3, -1.8]	38	0.9 [0.8, 1.1]	38

Variables are expressed as mean [95% CI]. BL, baseline; FU1, follow-up at 1 year; FU2, follow-up at 2 years; PSSR, peak systolic strain rate; PEDSR, peak early diastolic strain rate.

Table C2: Strain outcomes of surviving versus deceased patients.

	Circumferential				Radial		Longitudinal		
	Surviving	n	Deceased	n	Surviving[1]	Deceased[1]	Surviving	n	Deceased[1]
Global									
BL	-32.8 [-34.6, -31.1]	47	-32.7 [-36.0, -29.5]	18	55.3 [50.5, 60.1]	58.8 [51.3, 66,4]	-21.1 [-22.4, -19.8]	49	-20.0 [-21.3, -18.5]
FU1	-33.6 [-35.6, -31.8]	36	-33.8 [-37.2, -30.5]	12	58.5 [54.0, 63.7]	56.0 [45.2, 66.9]	-20.0 [-21.6, -18.4]	38	-20.3 [-22.1, -18.5]
FU2	-34.5 [-36.2, -33.0]	30	-36.8 [-43.5, -30.1]	8	64.0 [57.8, 71.3]	64.9 [47.6, 82.2]	-20.3 [-22.0, -18.8]	30	-21.1 [-24.1, -18.1]
PSSR									
BL	-2.1 [-2.3, -1.8]	47	-1.9 [-2.1, -1.6]	18	2.0 [1.8, 2.2]	1.9 [1.6, 2.1]	-1.1 [-1.2, -1.0]	49	-1.0 [-1.2, -0.9]
FU1	-1.9 [-2.1, -1.8]	36	-2.0 [-2.4, -1.7]	12	2.0 [1.8, 2.1]	1.9 [1.6, 2.1]	-1.0 [-1.1, -0.9]	38	-1.1 [-1.2, -0.9]
FU2	-2.0 [-2.2, -1.8]	30	-2.3 [-2.8, -1.7]	8	2.1 [1.9, 2.3]	2.1 [1.7, 2.6]	-1.0 [-1.1, -0.9] *	30	-1.2 [-1.6, -0.9]
PEDSR									
BL	2.0 [1.7, 2.2]	47	1.6 [1.1, 2.0]	18	-1.9 [-2.2, -1.7]	-1.5 [-2.0, -1.1]	1.1 [0.9, 1.2] *	48	0.7 [0.5, 1.0]
FU1	1.9 [1.7, 2.1]	36	1.8 [1.4, 2.2]	12	-1.9 [-2.1, -1.7]	-1.6 [-2.0, -1.2]	1.0 [0.8, 1.2]	38	0.8 [0.7, 0.9]
FU2	2.0 [1.8, 2.2]	30	1.9 [1.2, 2.5]	8	-2.1 [-2.4, -1.9]	-1.8 [-2.6, -1.0]	0.9 [0.8, 1.0]	30	1.1 [0.9, 1.3]

Variables are expressed as mean [95% CI]. BL, baseline; FU1, follow-up at one year; FU2, follow-up at two years; PSSR, peak systolic strain rate (1/s); PEDSR, peak early diastolic strain rate (1/s). [1] same number of patients as in circumferential direction * p-value < 0.05 for comparing parameters of surviving versus deceased patients with the independent t-test.

Survival analysis

Table C3: Receiver operating characteristic curve analysis with cutoffs determined for variables at FU1 with AUC > 0.600.

Variable	AUC	Cutoff	Sensitivity (%)	Specificity (%)	p-value
Volumetric imaging					
LVMi	0.502	-	-	-	-
LVEF	0.698	0.750	0.342	78.9	0.016
CI	0.497	-	-	-	-
LVEDVi	0.629	0.667	0.784	59.2	0.028
LVESVi	0.697	0.833	0.653	16.3	0.023
MCF	0.447	-	-	-	-
LVM/EDV	0.568	-	-	-	-
Strain imaging					
GCS	0.484	-	-	-	-
GRS	0.556	-	-	-	-
GLS	0.414	-	-	-	-
cPEDSR	0.514	-	-	-	-
rPEDSR	0.606	-1.71	0.500	0.667	0.306
lPEDSR	0.614	0.98	0.833	0.474	0.058
cPSSR	0.451	-	-	-	-
rPSSR	0.569	-	-	-	-
lPSSR	0.382	-	-	-	-

p-values determined from Kaplan-Meier analysis. AUC, area under the curve; CI, cardiac index; cPEDSR, circumferential peak early diastolic strain rate (PEDSR); cPSSR, circumferential peak systolic strain rate (PSSR); GCS, global circumferential strain; GRS, global radial strain; GLS, global longitudinal strain; LVEDVI, left ventricular end-diastolic volume index; lPEDSR, longitudinal PEDSR; lPSSR, longitudinal PSSR; LVEF, left ventricular ejection fraction; LVESVI, left ventricular end-systolic volume index; LVMI, left ventricular mass index; rPEDSR, radial PEDSR; rPSSR, radial PSSR.
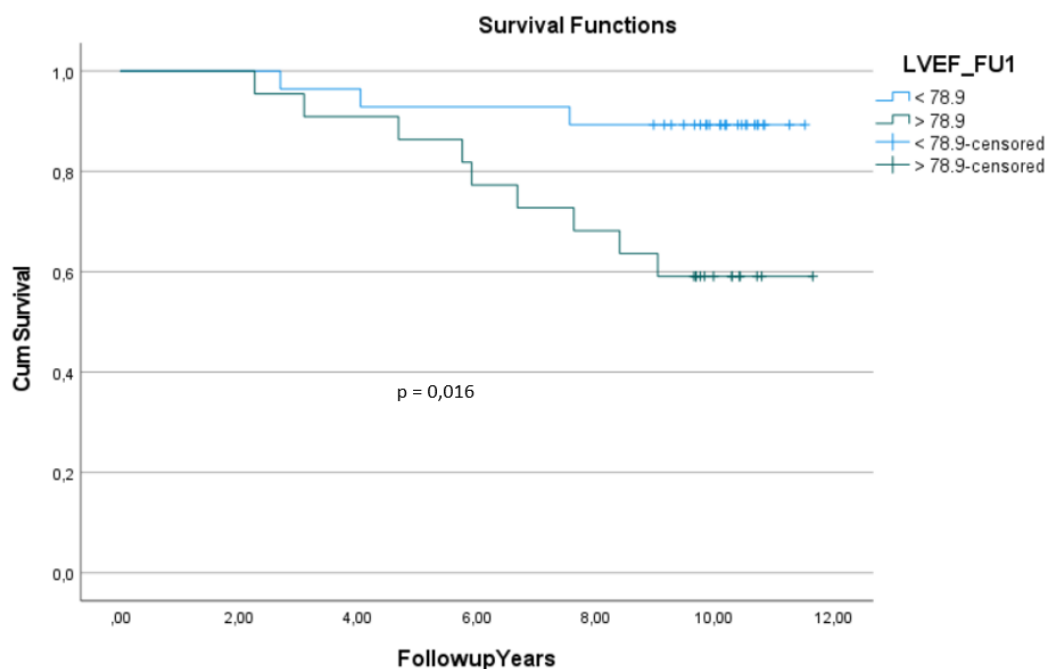

Figure C2: Kaplan Meier survival function based on left ventricular ejection fraction (LVEF) at 1 year follow-up (FU1).

Table C4: Receiver operating characteristic curve analysis with cutoffs determined for variables at FU2 with AUC > 0.600.

Variable	AUC	Cutoff	Sensitivity (%)	Specificity (%)	p-value
Volumetric imaging					
LVMi	0.408	-	-	-	-
LVEF	0.658	0.625	0.667	79.5	0.120
CI	0.623	2.93	0.750	0.581	0.083
LVEDVi	0.733	0.875	0.533	62.1	0.037
LVESVi	0.731	0.875	0.600	12.4	0.082
MCF	0.592	-	-	-	-
LVM/EDV	0.654	1.17	0.875	0.433	0.417
Strain imaging					
GCS	0.433	-	-	-	-
GRS	0.487	-	-	-	-
GLS	0.417	-	-	-	-
cPEDSR	0.513	-	-	-	-
rPEDSR	0.550	-	-	-	-
lPEDSR	0.333	-	-	-	-
cPSSR	0.371	-	-	-	-
rPSSR	0.458	-	-	-	-
lPSSR	0.317	-	-	-	-

p-values determined from Kaplan-Meier analysis. AUC, area under the curve; CI, cardiac index; cPEDSR, circumferential peak early diastolic strain rate (PEDSR); cPSSR, circumferential peak systolic strain rate (PSSR); GCS, global circumferential strain; GRS, global radial strain; GLS, global longitudinal strain; LVEDVI, left ventricular end-diastolic volume index; lPEDSR, longitudinal PEDSR; lPSSR, longitudinal PSSR; LVEF, left ventricular ejection fraction; LVESVI, left ventricular end-systolic volume index; LVMI, left ventricular mass index; rPEDSR, radial PEDSR; rPSSR, radial PSSR.
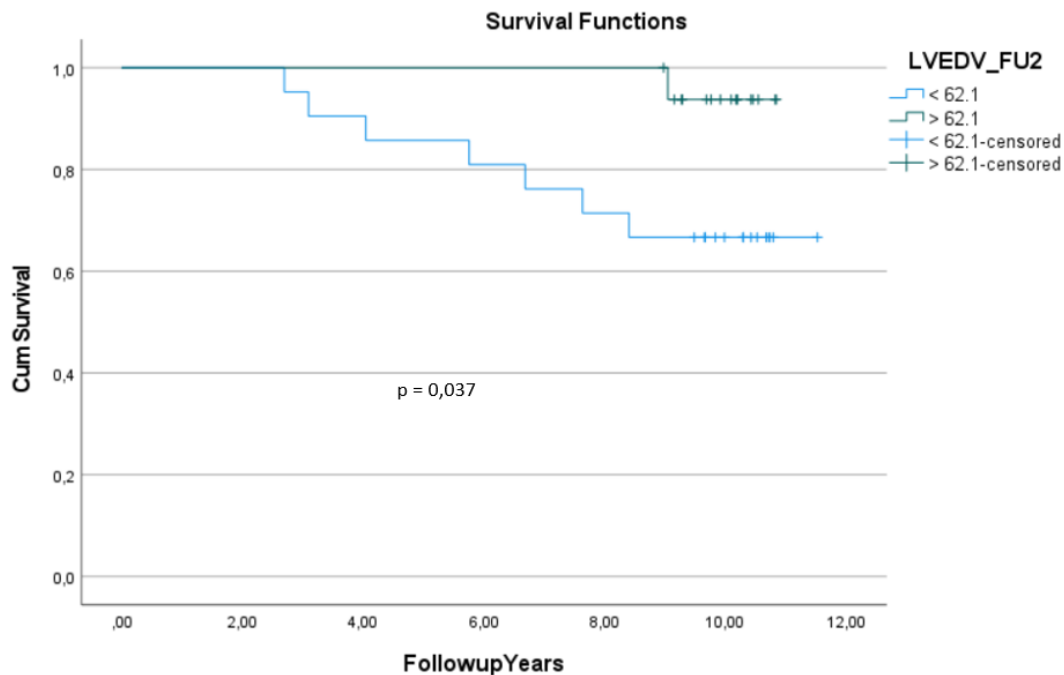

Figure C3: Kaplan Meier survival function based on left ventricular end-diastolic volume (LVEDV) at 2 years follow-up (FU2).

Strain outcomes of ALEGRO groups

Table C5: Global strain outcomes of the three ALEGRO groups.

	BL	n	FU1	n	FU2	n
GCS						
Group 1	-32.7 [-35.4, -30.6]	18	-32.9 [-35.1, -30.8]	15	-33.5 [-35.6, -31.4]	11
Group 2a	-31.5 [-34.3, -28.7]	25	-33.4 [-36.7, -30.1]	18	-36.0 [-39.7, -32.3]	13
Group 2b	-34.4 [-36.9, -31.8]	22	-34.6 [-37.5, -31.7]	15	-35.3 [-38.5, -32.1]	14
GRS						
Group 1	55.6 [46.0, 65.2]	18	57.2 [49.2, 65.1]	15	60.6 [48.7, 72.6]	11
Group 2a	55.4 [49.1, 61.9]	25	59.3 [52.0, 66.5]	18	71.0 [49.5, 82.5]	13
Group 2b	57.7 [51.3, 64.2]	22	56.9 [48.0, 65.8]	15	60.6 [50.9, 70.3]	14
GLS						
Group 1	-20.6 [-21.9, -19.2]	20	-20.8 [-23.7, -18.0]	15	-20.8 [-23.9, -17.7]	11
Group 2a	-20.3 [-21.9, -18.8]	25	-19.4 [-21.5, -17.3]	19	-19.4 [-22.0, -17.0]	13
Group 2b	-20.7 [-23.8, -18.8]	22	-20.0 [-21.8, -18.4]	16	-20.5 [-23.1, -19.0]	14

Variables are expressed as mean [95% CI]. BL, baseline; FU1, follow-up at 1 year; FU2, follow-up at 2 years; GCS, global circumferential strain; Group 1, steroid-free; Group 2a, standard; Group 2b, low-dose calcineurin inhibitor; GRS, global radial strain; GLS, global longitudinal strain.
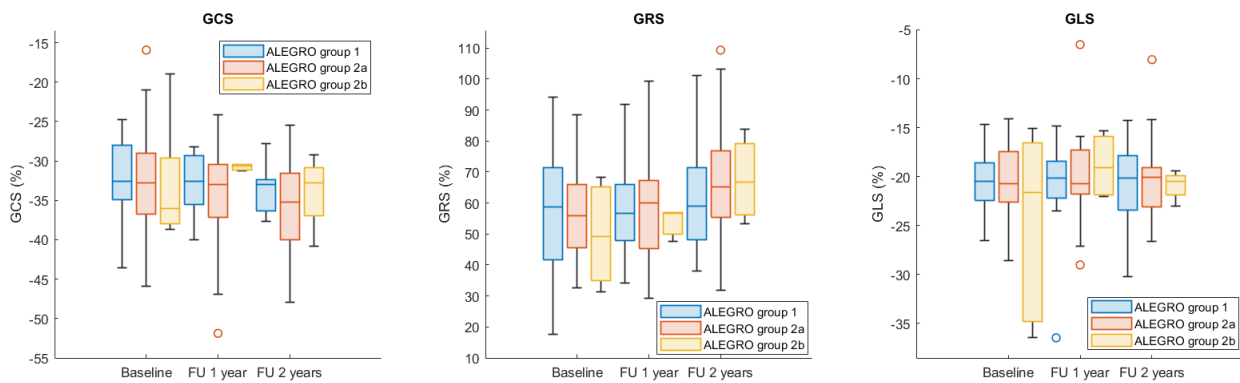

Figure C4: Boxplots of global strain results of different ALEGRO groups. GCS, global circumferential strain; FU, follow-up; Group 1, steroid-free; Group 2a, standard; Group 2b, low-dose calcineurin inhibitor; GRS, global radial strain; GLS, global longitudinal strain.

Table C6: Strain rate outcomes of three ALEGRO groups.

	PSSR						PEDSR		
	BL	n	FU1	n	FU2	n	BL[1]	FU1[1]	FU2[1]
Circumferential									
Group 1	-2.2 [-2.5, -1.8]	18	-1.9 [-2.1, -1.7]	15	-1.9 [-2.1, -1.7]	11	2.0 [1.5, 2.4]	1.7 [1.4, 2.1]	1.9 [1.5, 2.4]
Group 2a	-1.9 [-2.3, -1.6]	25	-2.0 [-2.3, -1.7]	18	-2.3 [-2.7, -1.9]	13	1.6 [1.3, 1.9]	1.8 [1.4, 2.1]	1.9 [1.4, 2.3]
Group 2b	-1.9 [-2.1, -1.7]	22	-2.0 [-2.3, -1.7]	15	-2.1 [-2.3, -1.8]	14	1.9 [1.7, 2.4]	1.8 [1.7, 2.3]	2.0 [1.8, 2.4]
Radial									
Group 1	2.0 [1.7, 2.4]	18	2.0 [1.8, 2.1]	15	2.0 [1.7, 2.3]	11	-1.9 [-2.4, -1.5]	-1.8 [-2.1, -1.4]	-2.0 [-2.5, -1.4]
Group 2a	1.9 [1.7, 2.2]	25	2.0 [1.7, 2.2]	18	2.3 [2.0, 2.6]	13	-1.6 [-1.9, -1.3]	-1.8 [-2.0, -1.5]	-2.0 [-2.5, -1.4]
Group 2b	1.9 [1.7, 2.2]	22	1.9 [1.7, 2.1]	15	2.0 [1.8, 2.3]	14	-2.0 [-2.3, -1.7]	-1.9 [-2.3, -1.6]	-2.1 [-2.4, -1.8]
Longitudinal									
Group 1	-1.1 [-1.3, -1.0]	20	-1.1 [-1.2, -0.9]	15	-1.0 [-1.2, -0.9]	11	1.0 [0.8, 1.3]	1.0 [0.7, 1.3]	1.0 [0.7, 1.2]
Group 2a	-1.1 [-1.2, -1.0]	25	-1.0 [-1.2, -0.9]	19	-1.0 [-1.3, -0.8]	13	0.9 [0.7, -1.1]	0.9 [0.6, 1.1]	0.9 [0.8, 1.1]
Group 2b	-1.1 [-1.3, -0.9]	22	-1.0 [-1.2, -0.9]	16	-1.0 [-1.1, -0.9]	14	1.0 [0.8, 1.2]	0.9 [0.8, 1.1]	0.9 [0.8, 1.1]

Variables are expressed as mean [95% CI]. BL, baseline; FU1, follow-up at 1 year; FU2, follow-up at 2 years; Group 1, steroid-free; Group 2a, standard; Group 2b, low-dose calcineurin inhibitor; PSSR, peak systolic strain rate; PEDSR, peak early diastolic strian rate. [1] same number of patients as for PSSR.
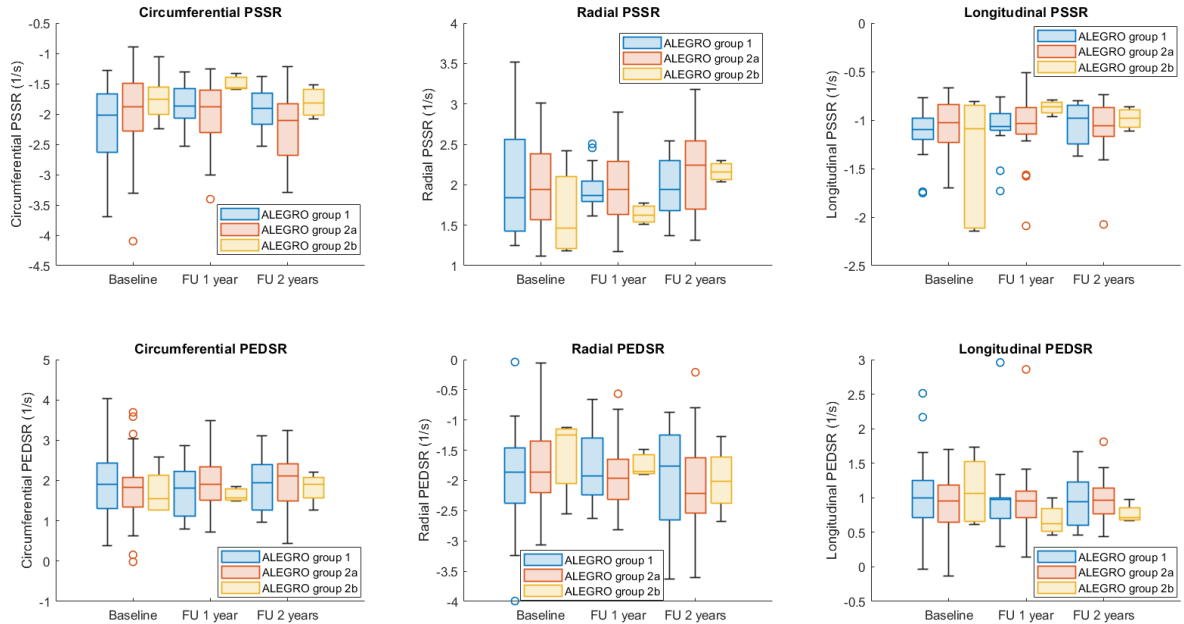

Figure C5: Boxplots of strain rate results of different ALEGRO groups. FU, follow-up; Group 1, steroid-free; Group 2a, standard; Group 2b, low-dose calcineurin inhibitor; PSSR, peak systolic strain rat; PEDSR, peak early diastolic strain rate.